Development of a novel fire following earthquake probabilistic framework applied to a steel braced frame

Patrick Covi [a], Nicola Tondini [a,*], Amir Sarreshtehdari [b], Negar Elhami-Khorasani [b]

[a] Department of Civil, Environmental and Mechanical Engineering, University of Trento, Via Mesiano 77, 38123 Trento, Italy
[b] Department of Civil, Structural and Environmental Engineering, University at Buffalo, NY 14260, USA

ARTICLE INFO

ABSTRACT

This paper describes a novel probabilistic fire following earthquake (FFE) framework to develop FFE fragility functions for steel braced frames. In particular, an 8-storey steel braced frame, located in a high seismic area, was used to demonstrate the framework. An algorithm was formulated to generate fire scenarios based on seismic damage. Damage caused by the earthquake was expressed in terms of inter-storey drift ratio (IDR) and peak floor acceleration (PFA). Damage was captured in structural and non-structural components, such as glazing and partition walls. In particular, floors with IDR and PFA that exceeded pre-defined thresholds were considered to experience ignition after an earthquake. More than 1100 nonlinear FFE analyses were performed by randomly generating values of window widths, fire load densities, earthquake intensities, and yield strength of steel at ambient and at high temperatures. Historic ground motions and natural fire curves were employed to characterize the hazards. Thermomechanical analyses were completed and failure criteria based on displacement and displacement rate were applied to the girders (primary beams) and columns. The results of simulations were processed to generate FFE fragility curves and surfaces for girder and column failures with respect to the time to failure in the FFE scenario and grouped based on spectral acceleration intervals. The results showed that the girder always failed first given the low structural redundancy due to the end conditions. Moreover, the higher the spectral acceleration, the more uniform the damage across the structure with a lower time to reach failure. It was finally found that the fire load density did not have a significant effect on the probability of failure for the case study under consideration.

1. Introduction

Fires following earthquake (FFE) have historically produced large post-earthquake damage [1,2]. Indeed, secondary triggered effects can strike an already weakened community and compound the damage. FFEs are a considerable threat as they can be widespread both at the building level and at the regional level within the affected area by the earthquake owing to the rupture of gas lines, failure of electrical systems, and at the same time, failure of the compartmentation measures inside buildings [3]. Moreover, FFEs are more difficult to tackle by the fire brigades because of the potential for a large number and extent of ignitions, disruptions within the infrastructural network that hinder timely intervention, and damage to the water supply system [4,5]. For instance, fires following the San Francisco 1906 earthquake caused 3,000 fatalities and major property losses with 28,000 buildings

destroyed for a value of approximately $250 million in 1906 dollars [2]. The post-earthquake fires caused by the 1923 Tokyo earthquakes lasted 3 days and caused 77% of the overall damage [6]. In both events, the damage caused by fires was greater than the damage due to the ground shaking. The 1995 Kobe earthquake also triggered about 140 fires, and the water flow and pressure remained functional only for 2 to 3 h after the earthquake to fight the fires [7]. The 1999 Turkey earthquake and 2011 Tohoku earthquake caused major fires, where the Tohoku earthquake fires lasted several days [8].

Passive and active fire protections can also get damaged by the earthquake and the fire can spread more rapidly within a building if compartmentation measures are compromised. For example, in 2011, the Christchurch earthquake caused severe damage to many secondary structural components, such as staircases, and non-structural components, such as façade systems, ceilings, interior walls, fireproofing

---

* Corresponding author.
E-mail addresses: patrick.covi@unitn.it (P. Covi), nicola.tondini@unitn.it (N. Tondini), amirsarr@buffalo.edu (A. Sarreshtehdari), negarkho@buffalo.edu (N. Elhami-Khorasani).

systems, etc. In general. failure of non-structural components has an impact on the building fire performance, such as (i) egress delay from the building; (ii) faster spread of fire; and (iii) quicker temperature rise in the structural elements due to damage in the fire protection system [9]. The structural fire performance can worsen significantly when the fire reaches an already damaged structure. In a performance-based approach, it would be sensible to evaluate the effect of an earthquake on the fire safety level of buildings in seismic-prone zones. However, no standard currently addresses this issue and the earthquake and fire actions are accounted for separately. Thus, there is a need to establish systematic analysis approaches for FFE to guide design decisions and prevent major disasters in the future.

Most of the existing literature on FFE involve numerical simulations of steel moment resisting systems with a few dedicated to steel braced frames. Talebi et al. [10] numerically studied the fire resistance of a steel braced frame, which was damaged due to a severe earthquake. The influence of two types of bracing systems, namely buckling restrained brace systems (BRBs) and conventional braces, on the overall stability of seismically damaged steel buildings to fire was investigated. Della Corte et al. [11] simulated the effect of FFE on an unprotected steel moment resisting frame. Miano et al. [12] assessed the seismic and fire response of an existing reinforced concrete building. Memari et al. [13] analysed the post-earthquake fire performance of moment resisting frames with reduced beam section connections. The study assumed a protected steel moment resisting frame with unprotected beam ends that experienced concentrated seismic damage. Behnam and Ronagh [14] studied the response of unprotected steel moment resisting frames under FFE. A pushover nonlinear analysis was performed in SAP2000 followed by the fire analysis on an equivalent-damaged frame in SAFIR. Elhami-Khorasani et al. [15] developed a framework for evaluating the post-earthquake fire performance of a steel moment resisting frame considering uncertainties.

At the material level, Sinaie et al., [16] proposed stress–strain relationships at elevated temperature based on Bézier curves for cyclically-damaged mild steel. Depending on the temperature and the amplitude of previously applied strain cycles, the stress–strain relationships at elevated temperatures were derived and validated against experimental tests on material coupons. At the element or component level, Braxtan et al. [17] conducted a series of tests on the seismic performance of sprayed fire-resistive material applied to steel elements. Damage to the fireproofing was observed after quasi-static cycling loading. The post-earthquake performance of the steel beam-to-column joint was then analysed numerically because of the limitations in the lab facility to perform fire tests on the seismically damaged specimens. Following this work, the same research group [18] investigated the post-earthquake fire response of a protected steel moment-resisting frame.

Few attempts have been carried out to experimentally investigate the effect of an earthquake on the fire performance of structural and non-structural components. In particular, Pucinotti et al [19,20] tested the post-earthquake fire behaviour of beam-to-concrete filled steel tube column joints. The low-cycle fatigue tests were performed at the lab facility of the University of Trento, whereas the fire tests were followed at the Building Research Establishment (BRE) in the UK. Since it was not practical to deliver the seismically-damaged specimens to the UK, specimens at the BRE were pre-damaged before being subjected to fire loadings by imposing monotonic loads equivalent to damage levels induced by the seismic loading. A full-scale test on a 3 m × 3 m × 3 m reinforced concrete frame has been recently performed by Kamath et al. [21] to investigate its fire performance after a seismic event. The seismic loading was imposed by actuators according to a predefined cyclic loading history. The fire was then applied in the form of a pool fire by using kerosene oil as the fuel. A large-scale test was carried out at the UCSD (University of California San Diego) [22,23] to study the post-earthquake fire performance of a 5-storey reinforced concrete building. The multi-storey structure was mounted on the shaking table and tests with seismic isolation and fixed-base were performed. Peak

accelerations up to 0.8 g and peak inter-storey drift ratios of up to 6% were reached during the strongest fixed-base motion. The subsequent fire tests were mainly conceived to check the impact of smoke and how the non-structural components performed after an earthquake. Fires ranged from 500 kW to 2000 kW.

The Performance-Based Earthquake Engineering (PBEE) framework requires probability relationships for Damage Measures (DMs) conditioned on Engineering Demand Parameters (EDPs) [24,25]. The EDP-DM relationships in the form of seismic fragility functions of non-structural components can be exploited for the development of a probabilistic framework to produce FFE fragility functions. The development of fire fragility functions has attracted recent interest among the fire research community. In particular, Gernay et al. [26,27] proposed a methodology to define fire fragility functions for a steel building exposed to compartment fires considering different fire loads. Lange et al. [28] and Shrivastava et al. [29] modified and adapted the widely used Performance-Based Earthquake Engineering (PBEE) approach for fire engineering [30]. Randaxhe et al. [31] proposed a probabilistic fire demand model for steel pipe-racks exposed to localized fires.

Existing probabilistic frameworks for FFE make simplifications in the fire development process, including the spread of fire within and between storeys, and the characterization of seismic damage for a seamless transition between earthquake and fire. Memari and Mahmoud [32] focused on the development of a framework for fragilities for steel moment frames subjected to fire following earthquakes but only considered damage to structural components with no consideration of non-structural components.

The aim of this work is to propose a novel methodology to derive FFE fragility functions for structural damage at the building level considering earthquake damage to structural and non-structural components and demonstrate the approach by application to a concentrically braced steel frame. The methodology takes into account the main sources of variability related to the seismic and fire actions (including fire spread within the building) as well as the mechanical responses owing to earthquake and fire. The paper is organised as follows: Section 2 describes the FFE framework and Section 3 presents the case study. In Section 4, the main outcomes along with discussion of results are highlighted and finally, the conclusions with the future perspectives are presented in Section 5.

2. FFE framework

The FFE probabilistic framework has been conceived to incorporate the main sources of variability into the analysis so that fragility functions, that are representative of the structural behaviour under FFE scenarios, could be generated. The framework is fully nonlinear since it both includes the material and the geometric nonlinearities and the analysis is sequential with the seismic analysis that influences the fire analysis but not the contrary. The framework consists of the following steps: (i) the nonlinear dynamic analysis is first performed; (ii) the fire development is carried out at specific locations in the building depending on the results of step (i) and the dynamic structural response; (iii) the thermomechanical analysis of the structural system is then completed.

2.1. Methodology

The major steps for implementing the FFE probabilistic framework are illustrated in Fig. 1. The process is followed to perform probabilistic FFE analyses and to obtain sufficient data to build fragility curves and surfaces. The framework is developed and implemented using a combination of different software, i.e. OpenSees [15,37], Ozone [38], and MATLAB [39]. The seismic analyses and the FFE structural analyses were performed in OpenSees. The zone model software Ozone [38] was used for the fire development analyses, whereas a specific code developed in MATLAB was exploited for the heat transfer analyses.
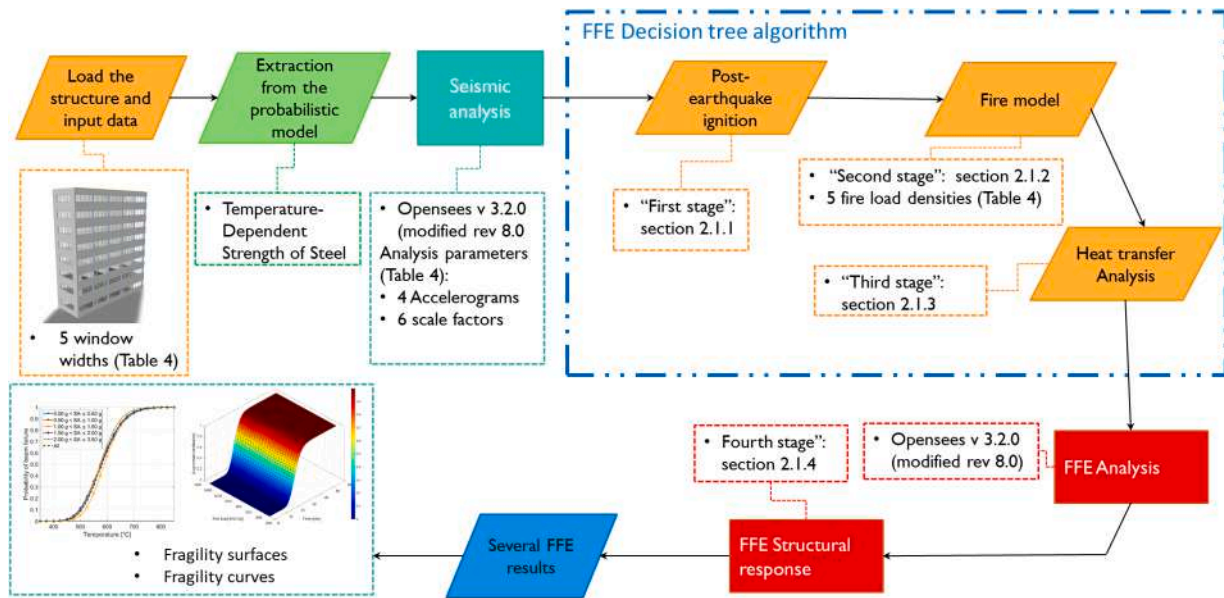
Fig. 1. Major steps in the implemented FFE framework.

The geometry of the structural system, cross section sizes, material properties, and applied loads are first defined in a Tcl script. Probabilistic parameters required for the analysis, such as compartment properties, are next generated. Once all the inputs and random variables are defined, the gravity and seismic analyses are performed. Then, OpenSees enters a "standby mode" and a background MATLAB process executes the FFE decision tree algorithm to automatically generate fire scenarios based on the seismic analysis results, in which the temperature of the hot

deterministic base and provides a probabilistic function for steel retention factor $k_{y,\,2\%,\,T}$ (Eq. (1)) by fitting to a dataset of measured retention factors. The function includes the effect of strain hardening and is relatively easy to implement in a finite element software. The variance in the retention factor is captured using the random variable ε, which follows the standard normal distribution function. The same function is used to generate random values of yield strength for ambient and high temperatures.

$$k_{y,2\%,T} = \frac{1.7 \times \exp\left[\text{logit}\left(\widehat{k}^*_{y,2\%,T}\right) + 0.412 - 0.81 \times 10^{-3} \times T + 0.58 \times 10^{-6} \times T^{1.9} + 0.43 \times \varepsilon\right]}{\exp\left[\text{logit}\left(\widehat{k}^*_{y,2\%,T}\right) + 0.412 - 0.81 \times 10^{-3} \times T + 0.58 \times 10^{-6} \times T^{1.9} + 0.43 \times \varepsilon\right] + 1}$$

(1)

gases in the compartments is computed using Ozone. Heat transfer is then conducted in MATLAB, followed by the structural analysis at elevated temperatures in OpenSees. Finally, the generated results are used to construct the fragility functions.

In the established framework, a suitable stress–strain constitutive material model for steel has to be selected, given the nonlinear nature of the FFE analyses, and keeping in mind that the outcomes have to be accurate both for the seismic and thermomechanical analyses. In particular, this applies to the bracing system that could be affected both by damage from inelastic hysteretic behaviour and thermal attack. Thus, the material model should enable a seamless transition between the seismic and thermomechanical analyses, considering damage at the end of the dynamic analysis. A custom material class, i.e., SteelFFEThermal, was developed for nonlinear FFE analyses in OpenSees. The Steel-FFEThermal material has the same definition as the Giuffrè-Menegotto-Pinto uniaxial steel stress–strain model at ambient temperature. However, when the temperature is applied, the material class switches the constitutive law to the stress–strain constitutive law for steel at elevated temperature as for EN 1993-1-2 [34]. A detailed explanation of the material class can be found in [33].

The yield strength of steel f_y at ambient (seismic analysis) and high temperatures (fire analysis) was modelled as a random variable using a continuous logistic function [35,36]. The formulation uses the EN1993-1-2 [34] steel model for yield strength at high temperatures as a

where $\text{logit}\left(\widehat{k}^*_{y,2\%,T}\right) = \ln\left(\frac{\widehat{k}^*_{y,2\%,T}}{1-\widehat{k}^*_{y,2\%,T}}\right)$, $\widehat{k}^*_{y,2\%,T} = \frac{\widehat{k}_{y,2\%,T}+10^{-6}}{1.7}$, and $\widehat{k}_{y,2\%,T}$ is

the temperature-specific retention factor as prescribed by EN1993-1-2 [34].

2.1.1. First stage of FFE decision tree algorithm: Post-earthquake ignition

As previously indicated, a nonlinear time-history analysis is completed first. Once the seismic analysis is completed, inter-storey drifts and accelerations are recorded for every floor. OpenSees enters in a "standby mode" until the FFE decision tree algorithm generates the information for the fire analysis. Fig. 2 illustrates the schematic procedure of the first stage to identify floors with ignition. Then, a compartment within the floors where the ignition occurs is randomly selected following a uniform distribution. The FFE decision tree algorithm extracts the maximum inter-storey drifts and accelerations for each floor. The conditions to determine compartments with the likelihood of FFE are as follows:

- Condition A: the acceleration of at least one floor must be greater than or equal to 0.7 g.
- Condition B: the inter-storey drift ratio of at least one floor must be greater than or equal to 1.0%.

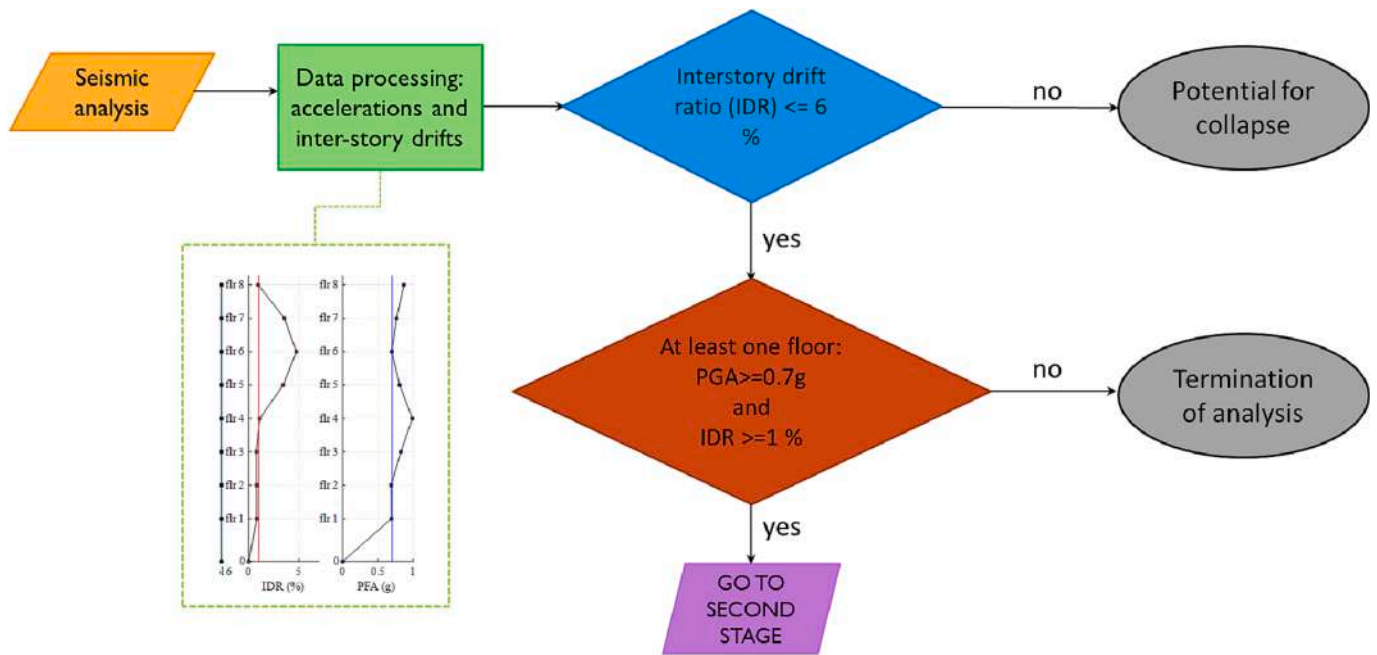It is worth pointing out that an "and" logical condition is applied

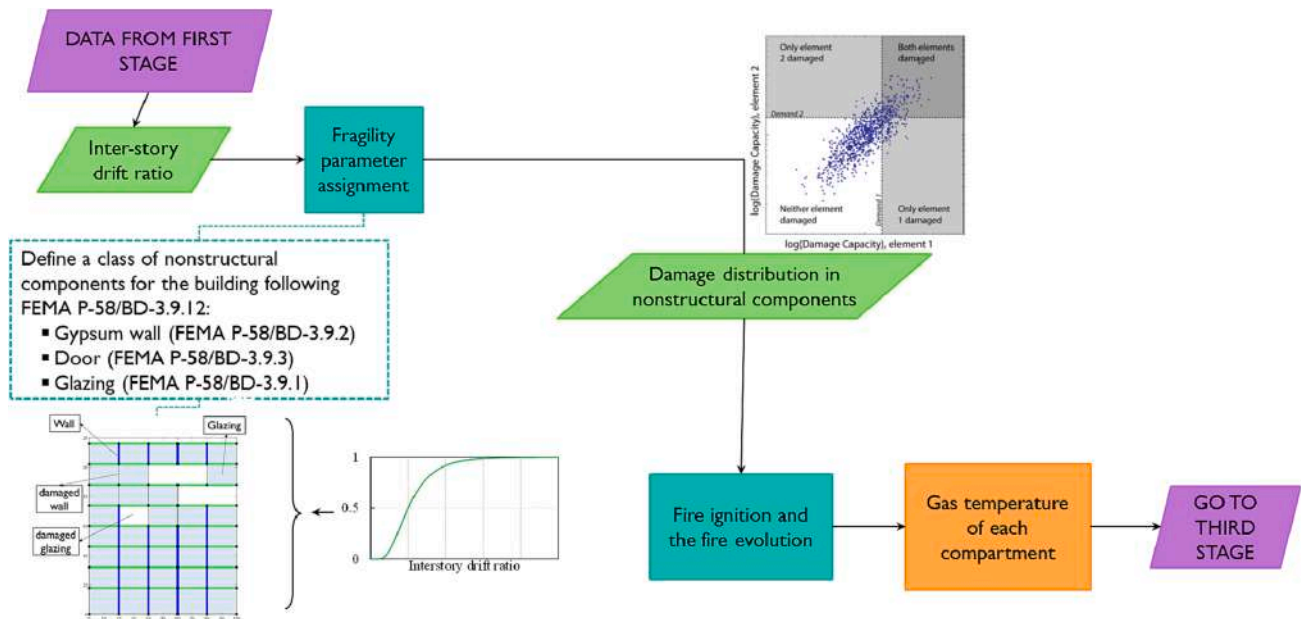**Fig. 2.** Scheme for the first stage: floors with ignition.

Fig. 3. Scheme for the second stage: fire model.

above, which means that both conditions have to be valid to ignite a fire within the building after an earthquake. The requirement is imposed based on observations in historic data.

Condition A is related to the likelihood of damage to the gas network in or near the building, such as leakage from a screw joint or mechanical joints that are the weakest points of the gas network. Ueno et al. (2004) [40] present a set of fragility functions for low-pressure gas facilities during the 1995 Kobe earthquake. They showed that a floor acceleration value of 0.7 g or above in steel buildings implies major damage, i.e., a 90% probability of occurrence of leakage or rupture to the low-pressure gas facilities.

Condition B is related to the likelihood of damage to the electrical services, which is a function of the inter-storey drift in the building. An

inter-storey drift ratio equal to 1.0% was chosen as a value between the life-safety limit state (0.5 %) and the collapse limit state (2.0%) for a braced steel frame based on FEMA P-356 [41]. Moreover, structural collapse due to the seismic event was assumed for an inter-storey drift ratio equal to or greater than 6%, i.e., three times the collapse limit state, at which point the decision tree algorithm terminates the analysis.

2.1.2. Second stage of FFE decision tree algorithm: fire model

Fig. 3 illustrates the schematic procedure of the second stage. Damage to the structural system can be minor, but the non-structural components (NSCs) could still experience damage that would affect the fire behaviour inside the building. Damage to components such as walls, partitions, and external glazing affects the fire compartmentation
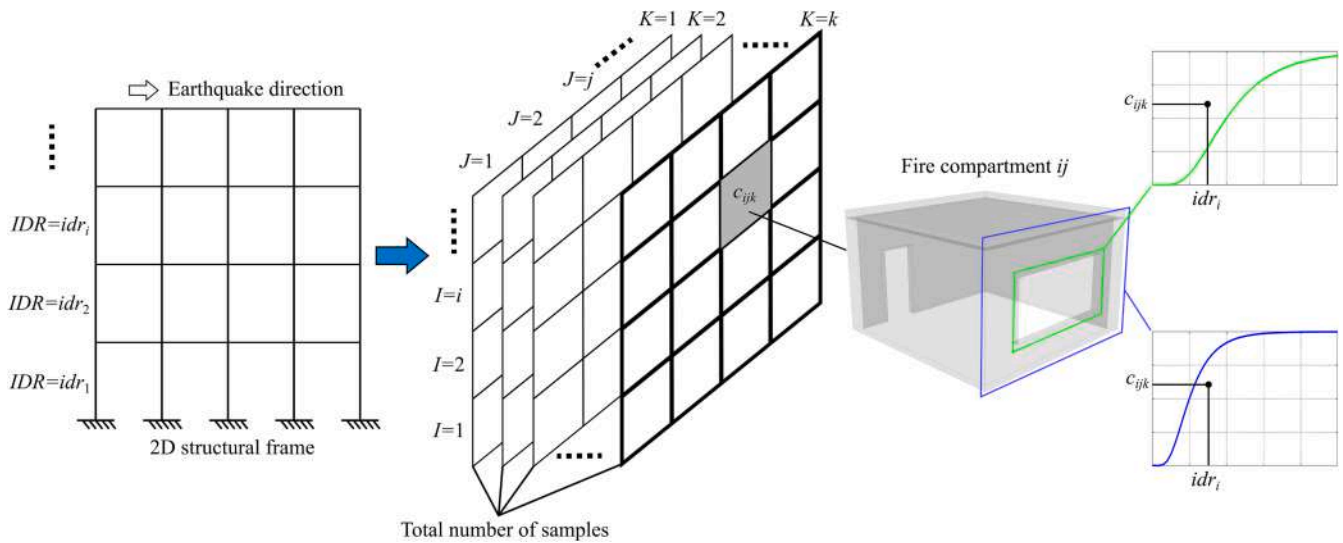
Fig. 4. Implemented process to determine the damage states for NSCs in a compartment considering uncertainties.

and ventilation leading to larger fires and an expedited room-to-room fire spread in one floor or along the height by "leap-frog" effect. In this study, the effect of damage to glazing, partition walls made of gypsum, and doors on the fire behaviour inside the building is considered. Damage to ceiling tiles for potential vertical fire spread is not considered. Sprinklers and any active firefighting measure to extinguish the fire are conservatively assumed not to be functional after the earthquake. Damage to NSCs, including glazing, partition walls, and doors, is quantified using the fragility functions provided in FEMA P58 [42] background documentation.

Glazing is a drift sensitive component. The fragility parameters for glazing are taken from the FEMA P-58 background document [43]. The document provides a comprehensive list of different glazing types and the corresponding fragility parameters for different damage states. There are three damage state classifications based on the type of glazing. The damage states are based on the observations made during experiments on different curtain walls and storefront glazing types. The experiments looked into glasses with different types (annealed, heat strengthened, fully tempered), configuration (monolithic, insulating glass unit, asymmetric insulating glass unit), sizes, glass to frame clearance, framing type, thickness, and width-to-height ratio. Generally, the type of glass determines the damage state classifications. For the purpose of this study, each damage state is evaluated based on whether or not it will influence the fire behaviour in the building. Thus, only those damage states that lead to the loss of integrity of glass (i.e., glass damage and glass fallout) are included. According to AAMA 501.6 [44], the "glass fallout" is defined as cases when at least 6.45 cm^2 (1 in^2) of the glass panel is fallen out. There is no information available on the specific size of damaged glass pieces or fallout; therefore, it is assumed that the full window is open or broken for the purpose of fire modeling when the "glass fallout" damage state is selected.

Partition walls made of gypsum are also drift sensitive components. Damage to gypsum walls is classified using three damage states as a function of the IDR [45]. The damage states are defined based on the repair method, and to some extent, engineering judgment. The only damage state that affects compartmentation, and thus the rate of fire spread, is the one when the gypsum walls, studs, tracks, and steel framing undergo severe damage. The fragility functions for the partitions provide the exceedance probability of a damage state along the earthquake direction. A partition wall perpendicular to the direction of the earthquake is assumed to be damaged when both adjacent partition walls in the direction of earthquake are damaged.

Doors can be open or closed. Thus, their status can change the ventilation conditions for the compartment. The door damage states in FEMA [46] depend on the level of earthquake damage to the door and hinges as a function of IDR. This was also highlighted in a recent experimental work [47]. However, it is still difficult to accurately correlate the damage to the open or closed condition of the door after the earthquake. Therefore, the door status is generated as a random binary number independently of the level of seismic intensity.

The procedure to quantify the level of damage to the designated fire compartments is shown in Fig. 4. The fire compartments in the building are defined with respect to bays and floors of the structural system, where each bay in a floor is a fire compartment. The status of a compartment is based on the combined conditions of the glazing, partition walls, and doors.

The likelihood of a fire compartment to reach a damage state given the level of earthquake intensity is characterized by a randomly generated variable c_{ijk} where i, j, and k represent floor number, bay number, and the sample number, respectively. The random variable c_{ijk}, which represents the compartment state, has a value between zero and one. The c_{ijk} is compared with the brackets of the probability of exceedance derived from the fragility functions in FEMA P-58 [42] to determine the damage state given the level of earthquake intensity. The compartment state variables c_{ijk} for all the bays in a given floor are correlated using the correlation coefficient matrix ρ_{ij}. The correlation is defined based on the relative separation distance of every two compartments, i.e., nearby compartments display more similarity in the level of experienced damage. In general, historical events and experimental observations can be used to establish such correlations; however, it is beyond the scope of this research to study damage correlations between compartments. Thus, the correlation coefficient for two adjacent compartments is considered as 0.5. The correlation matrix ρ for floor i is an $n \times n$ matrix, where n is the number of bays in a floor and has the form of Eq. (2). More detailed discussions on the difference between cases with and without correlation are presented in [48].

$$\rho = \begin{bmatrix} 1 & 0.5 & 0 & \cdots & 0 \\ 0.5 & 1 & 0.5 & 0 & \vdots \\ 0 & 0.5 & \ddots & \ddots & 0 \\ \vdots & 0 & \ddots & 1 & 0.5 \\ 0 & \cdots & 0 & 0.5 & 1 \end{bmatrix}_{n \times n} \tag{2}$$

A uniformly distributed Latin Hypercube Sampling (LHS) technique with the reduced spurious correlation [49] is implemented to randomly
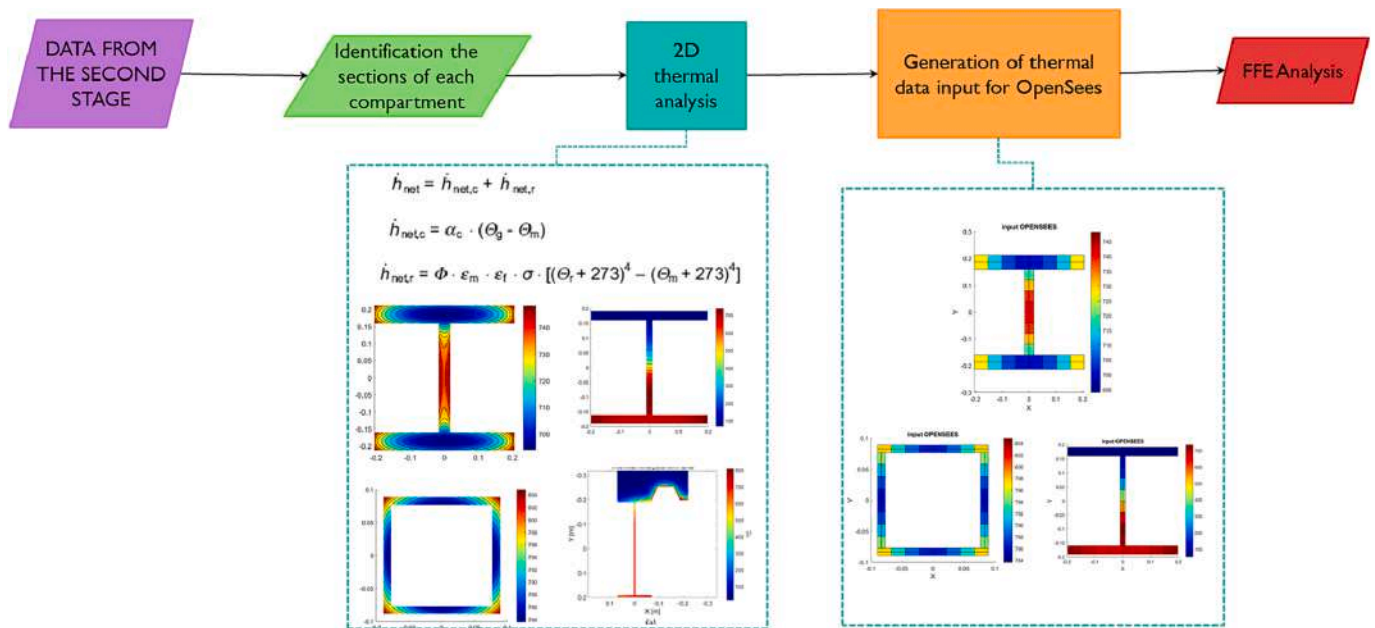
Fig. 5. Scheme for the third stage: identification of the steel sections in each compartment.

generate the random variable c_{ijk}. A Cholesky decomposition process is utilized where the input matrix must be positive definite. Thus, the matrix is substituted with the corresponding systemic nearest semi-definite matrix to ensure a positive definite condition [50]. This process expedites the correlation convergence for a smaller number of samples to save computational cost.

A fire is initiated in a compartment that is randomly selected following a uniform distribution on each floor with the IDR and PFA larger than the defined thresholds. The time–temperature curve and characteristics of the fire behaviour in fire compartments are quantified using OZone [38]. The time–temperature is based on the variability in fire load density ($q_{f,d}$), opening size, and the condition of glazing and doors. The opening size is a function of both doors and windows. Fire spread in the vertical direction follows an upward direction and the compartment on the upper floor ignites when a compartment on the lower floor reaches the flashover condition. The status of the partitions after the earthquake (damaged or intact) influences the fire spread rate from one compartment to the adjacent compartment in the horizontal direction. The delay times for the fire spread between two compartments in the horizontal direction are taken as 30 and 15 min when the partition is intact and damaged, respectively.

2.1.3. Third stage of FFE decision tree algorithm: heat transfer analysis

It was not possible to automatically perform the thermal analyses inside OpenSees 3.2.0 [37]. The use of another independent software (i.e., SAFIR) was also not possible due to lack of compatibility with Linux operating systems, typically used for High-Performance Computing (HPC) in order to reduce the computational burden. Therefore, a MATLAB. Therefore, a MATLAB [39] script was developed and validated against SAFIR to perform thermal analyses.

Fig. 5 illustrates the schematic procedure of the third stage. The procedure creates a two-dimensional thermal finite element analysis for each compartment and automatically assigns the boundary conditions to each heated member of the selected compartment (columns, girders, beams, and braces) using cross-sections that are discretized with an appropriate mesh size. The thermal modeling of the girder and beam section includes the effective shape and width of the concrete slab. The applied fire curve is generated in the second stage.

Thermal action is determined by the net heat flux $\dot{h}_{net}$ to the surface

of the member. The net heat flux on the fire exposed surfaces is determined by considering heat transfer due to convection and radiation (Eq. (3)):

$$\dot{h}_{net} = \dot{h}_{net,c} + \dot{h}_{net,r} \tag{3}$$

where $\dot{h}_{net,c}$ is the net convective heat flux and $\dot{h}_{net,r}$ is the net radiative heat flux. The following equation provides the net convective heat flux (Eq. (4)):

$$\dot{h}_{net,c} = \alpha_c \cdot (\theta_g - \theta_m) \tag{4}$$

where:

- α_c is the coefficient of heat transfer by convection;
- θ_g is the gas temperature in the vicinity of the fire exposed member and was taken from the results of the fire development phase; and
- θ_m is the surface temperature of the member.

For simplicity, EN1991-1-2 (2002) [51] provides an approximation of the net heat flux (W/m^2) due to radiation as follows (Eq. (5)):

$$\dot{h}_{net,r} = \phi \cdot \varepsilon_m \cdot \varepsilon_f \cdot \sigma \cdot \left[(\theta_r + 273)^4 - (\theta_m + 273)^4 \right] \tag{5}$$

where:

- ϕ the configuration factor;
- ε_m is the surface emissivity of the member (0.7 for carbon steel according EN 1993-1-2);
- ε_f is the emissivity of the fire (it is taken in general as 1.0 according EN 1991-1-2 [34]);
- σ is the Stephan Boltzmann constant (5.67×10^{-8} W/m^{2}K^4);
- θ_r is the effective radiation temperature of the fire environment;
- θ_m is the surface temperature of the member.

The configuration factor ϕ is taken conservatively equal to 1.0. The thermal properties of steel and concrete were taken from EN 1993-1-2 [34] and EN 1992-1-2 [52], respectively, and were kept constant. A uniform room temperature of 20 °C is assigned to the sections as an initial condition.
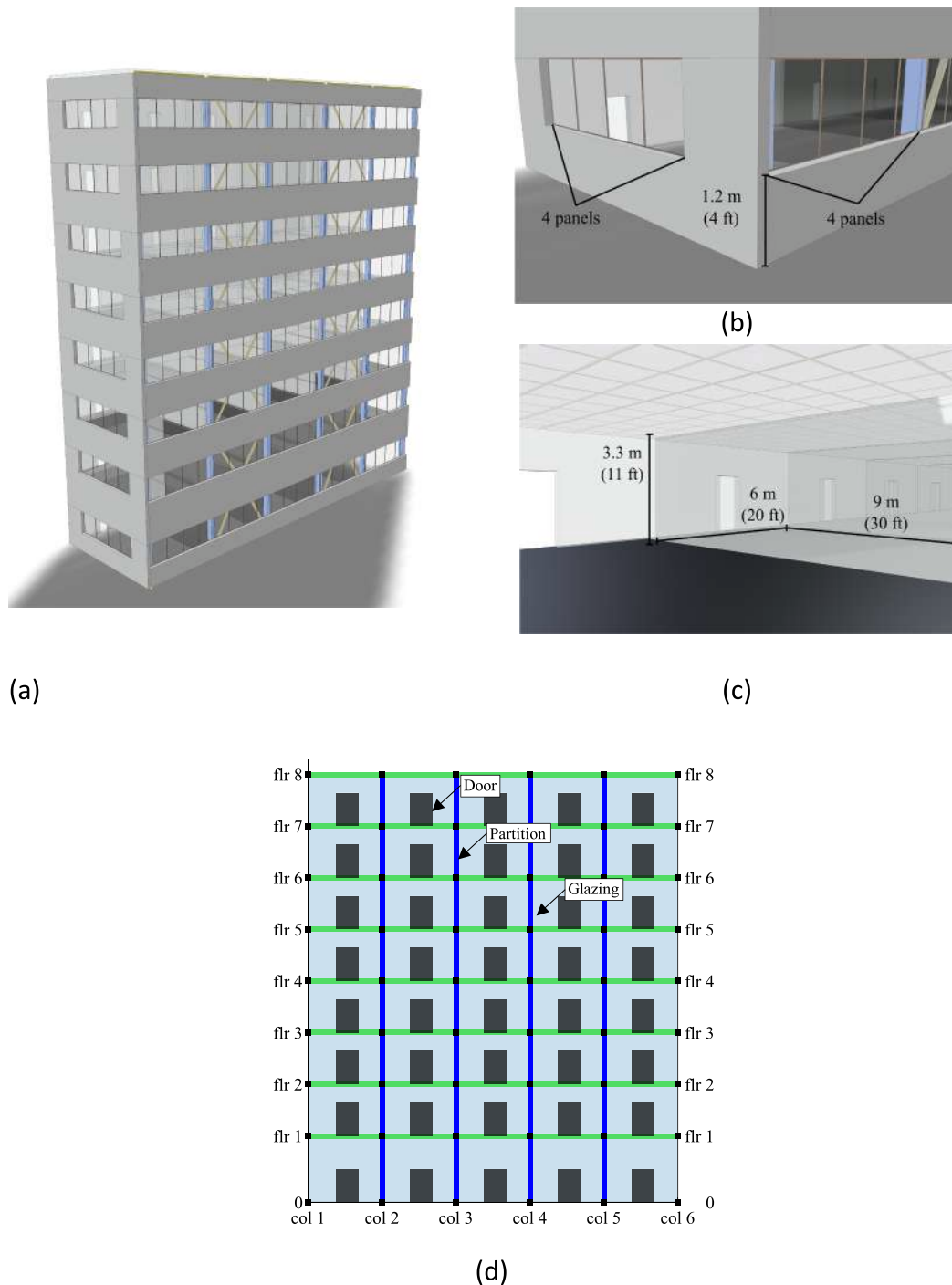
Fig. 6. (a) Isometric view of the building for the case study; (b) configuration of windows; (c) inside view of a compartment; (d) schematic representation of the prototype building with the non-structural components.

2.1.4. Fourth stage of FFE decision tree algorithm: FFE structural response

The FFE structural analysis is initiated once the heat transfer analysis for the selected FFE scenario is completed. Different limit states, following EN 1363-1 [53], are defined to identify failure in the structural members:

- Girders and beams - Limit state 1 (LS1):

  (i) deflection exceeding $L^2/400d$
  (ii) rate of deflection exceeding $L^2/(9000d)$ mm/min

- Columns - Limit state 2 (LS2):

  (i) vertical contraction exceeding $C = h/100$ mm
  (ii) rate of vertical contraction exceeding $dC/dt = 3\,h/1000$ mm/min
  Another limit state based on [26] was considered for the column that corresponds to a sudden increase in transversal deflection

- Columns - Limit state 3 (LS3):

  (i) rate of lateral deflection at mid-height 50 mm/min

where *h* is the initial column height in mm, *L* is the girder/beam length, and *d* is the depth of the girder/beam. It is worth pointing out that failure of a column may lead to the partial or global collapse of the building based on the degree of redundancy, whereas failure of a girder or a beam may not be as critical as a column failure.

3. Case study

3.1. Description

The methodology was applied to an eight-storey three-bay steel frame with concentric bracings in two central bays. This frame is part of an office building designed and presented in NIST Technical Note 1863-2 [54]. The building was designed in an area of high seismicity. For the purpose of this study, the city of Los Angeles was chosen for the FFE analyses. The structural members were considered as not protected against the thermal action. The plan dimensions for all floors and roofs were 46.33 m (152 ft) in the E-W direction, including five 9.14 m (30 ft) bays, and 31.01 m (102 ft) in the N-S direction, including five 6.10 m (20 ft) bays. The storey height was 4.28 m (14 ft) except for the first floor, which is 5.49 m (18 ft) high. The width of the windows for the structure were varied from 1.5 to 6 m (5 to 20 ft) with 1.5 m (5 ft) intervals. The windows had a constant sill height of 1.2 m (4 ft). Fig. 6a-c shows the view of the building with a window width of 6 m and Fig. 6d illustrates a schematic representation with the non-structural components. Note that the exterior bays are differentiated from the interior bays in terms of the number of window panels. The exterior bays have windows on two sides, i.e. parallel and perpendicular to the direction of the earthquake, while the interior ones have windows on one side only. The windows consist of four panels with a height of 1.8 m (6 ft) and a width of 1.5 m (5 ft) (i.e., the aspect ratio is 6:5). The type of glazing was taken as monolithic, non-laminated, annealed, and dry-sealed with a thickness of ¼ in and clearance of 10.9 mm (0.43 in). The median and dispersion of the glazing fragility function as a function of the inter-storey drift ratio were 0.0219 and 0.3, respectively [43]. If the glazing remained intact after the earthquake, it was assumed that the window would break during the fire with the opening size changing linearly as a function of fire temperature (50% of a window broken at 400 °C and 100% of a window broken at 500 °C).

Fig. 6c shows the inside view of the compartments with the positioning of the doors inside each compartment and how the interior space is partitioned. The height and width of doors for each compartment were 2 m (6.5 ft) and 0.9 m (3 ft), respectively. The thickness of interior partitions was 20 cm (8 in), including the gypsum board. The floor system consisted of 15 cm (6 in) thick normal weight concrete. The median and dispersion of the partition wall fragility function as a function of the inter-storey drift ratio were 0.012 and 0.45, respectively [45]. The height of the fire compartment was 3.3 m (11 ft), which was different from the structural system floor height. The height of the fire compartment was calculated by excluding the height of the slab, the height of the girder and the other mechanical equipment (i.e., pipes, heating system) that are typically installed at the ceiling level. Note that the fire compartment height for the first and remaining floors was kept similar. Table 1 lists the probability distributions and the corresponding parameters for glazing, partition walls, and door.

The following structural material types and corresponding nominal properties were assumed in the design:

- Wide-Flange Sections: A992 Grade 50, Yield strength $F_y = 345$ MPa (50 ksi), $R_y = 1.1$ (ratio of the expected yield strength to the specified minimum yield stress of the material).
- Hollow square sections (HSS): A500 Grade B, $F_y = 317$ MPa (46 ksi), $R_y = 1.4$
- Young's modulus: $E = 200{,}000$ MPa (29,000 ksi), Shear module: $G = 77{,}221$ MPa (11,200 ksi), Poisson's ratio: $\eta = 0.3$

The yield strength of steel F_y for all the elements was taken as a random variable following the logistic function of Eq. (1) using LHS.

The design loads were based on ASCE 7-10 [55]. The floor and roof dead load consisted of the weight of the steel members, metal deck, and concrete slab. A total dead load of 2.92 kN/m^2 (61 psf), comprising the self-weight of the floor slab and the superimposed load, and a live load of 2.39 kN/m^2 (50 psf) was applied to each floor except for the roof level. Indeed, on the roof, the total dead and live loads values were taken as 2.68 kN/m^2 (56 psf) and 1.44 kN/m^2 (30 psf), respectively. A 3.65 kN/m (250 plf) superimposed dead load was also applied to the horizontal perimeter to account for the facade (curtain wall) weight. The design seismic loads were considered according to the Equivalent Lateral Force (ELF) and Response Spectrum Analysis (RSA) procedures in ASCE 7-10 [55].

Fig. 7 shows the member sizes and the location of the N-S perimeter frame, selected for the analysis. Fig. 7 also shows the gravity loads acting simultaneously with the seismic load and the fire load.

The following parameters summarize the seismic hazard used for the design:

- Building Risk Category: II
- Site Soil Conditions: Site Class D, Stiff Soil according to the ASCE 7-10 Table 20.3-1 [55].
- Spectral Response Acceleration Parameters: listed in Table 2.
- Seismic Design Category (SDC): D taken as D_{max} as used in FEMA P-695 [56].

3.2. Ground motions and fire load densities

In this section, the quantities that characterized the earthquake and fire hazards, i.e., the time-history accelerograms and fire load densities, are described for the case study under consideration. In particular, the suite of far-field records, that was selected as the input motion database, consisted of 22 records (each with two horizontal components) following FEMA P-695 [56,57]. From the far-field records, 14 of the 44 horizontal component records were selected as the ground motion set for the FFE analyses. The accelerograms were modified to match the target spectrum in the period range of $0.2T_1$ and $1.5T_1$, where T_1 is the fundamental period of the structure that was equal to 1.50 s. Table 3 summarizes the 14 strong motion records used for the N-S direction in the FFE analyses, including the magnitude and peak ground acceleration. The listed ID in the table corresponds to the same numbering given in FEMA P-695 [56,57]. Fig. 8 illustrates the set of acceleration response spectra, original and scaled, and the scaled average response spectrum. In the probabilistic analysis, 6 scale factors were applied to the accelerograms: 0.50; 0.75; 1.00; 1.25; 1.50; 1.75.
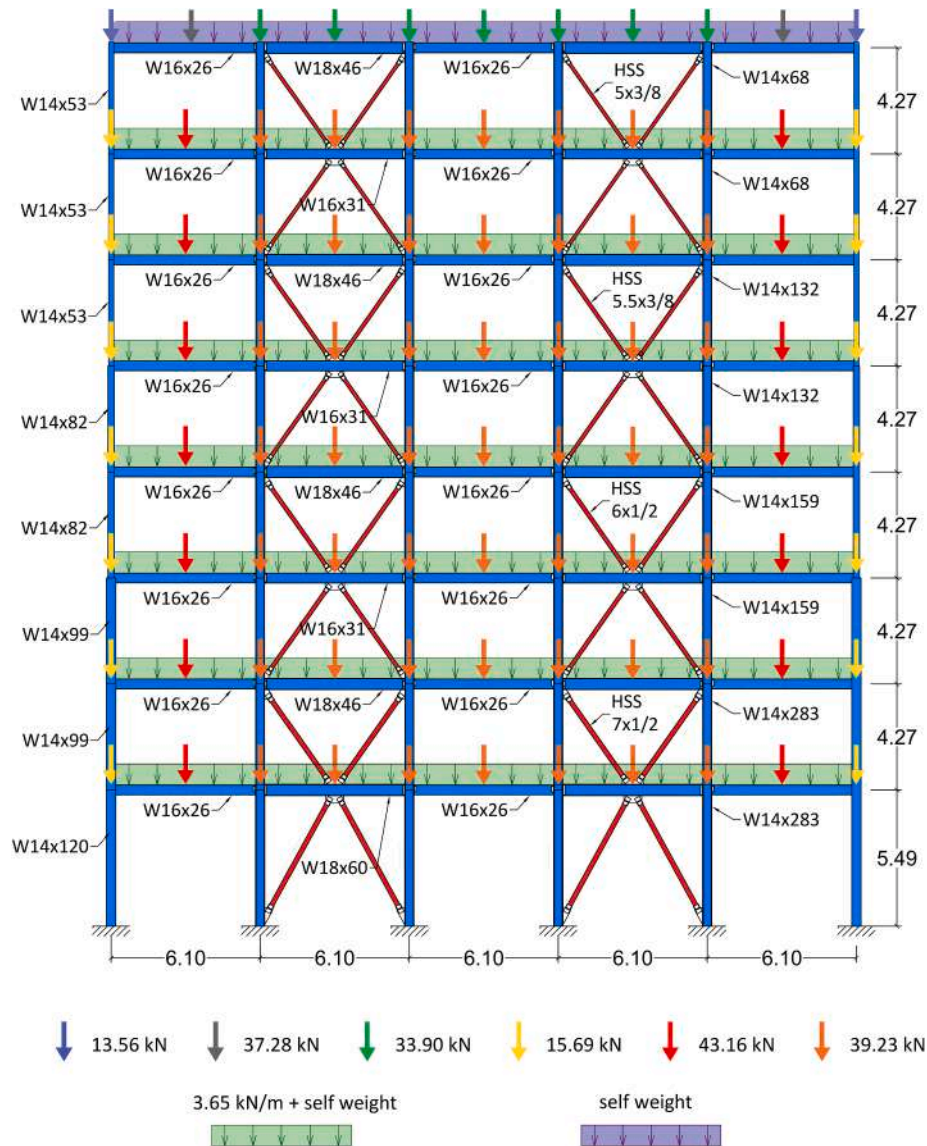
Table 1

Probability distributions for the non-structural components.

Component	Distribution	Parameter
Glazing	Lognormal	Inter-storey drift ratio $\mu = 0.0219$, $\sigma = 0.30$
Partition walls	Lognormal	Inter-storey drift ratio $\mu = 0.0120$, $\sigma = 0.45$
Door	Discrete uniform	Open or closed{0,1}

Fig. 7. Configuration of the frame. Dimensions in m.

Table 2
Spectral Response Acceleration Parameters.

SDC	Description	D_{max}
S_s	Spectral response acceleration parameter at short periods	1.5 g
S_1	Spectral response acceleration parameter at a period of 1 s	0.6 g
F_a	Short period site coefficient	1.0
F_v	Long period site coefficient	1.5
$S_{MS} = F_a S_s$	Spectral response acceleration parameter for short periods	1.5 g
$S_{M1} = F_a S_1$	Spectral response acceleration parameter at 1 s period	0.9 g
$S_{DS} = \frac{2}{3} S_{MS}$	Design earthquake spectral response acceleration parameter at short period	1.0 g
$S_{D1} = \frac{2}{3} S_{M1}$	Design earthquake spectral response acceleration parameter at 1 s period	0.6 g
3.5 T_s	$T_s = S_{D1}/S_{DS}$	2.1 s

Table 3
Accelerogram set.

ID	Event name	Station	Year	Mw	PGA (g)
1	Northridge, USA	Beverly Hills - Mulhol	1994	6.7	0.52
2	Northridge, USA	Canyon Country-WLC	1994	6.7	0.48
3	Duzce, Turkey	Bolu	1999	7.1	0.82
5	Imperial Valley, USA	Delta	1979	6.5	0.35
6	Imperial Valley, USA	El Centro Array #11	1979	6.5	0.38
8	Kobe, Japan	Shin-Osaka	1995	6.9	0.24
9	Kocaeli, Turkey	Duzce	1999	7.5	0.36
10	Kocaeli, Turkey	Arcelik	1999	7.5	0.22
11	Landers, USA	Yermo Fire Station	1992	7.3	0.24
14	Loma Prieta, USA	Gilroy Array #3	1989	6.9	0.56
16	Superstition Hills, USA	El Centro Imp. Co.	1987	6.5	0.36
17	Superstition Hills, USA	Poe Road (temp)	1987	6.5	0.45
18	Cape Mendocino, USA	Rio Dell Overpass	1992	7	0.55
19	Chi-Chi, Taiwan	CHY101	1999	7.6	0.44

The case study is an office building for which 5 values of fire load density were selected based on a discrete sampling uniform distribution, because fuel was an independent variable: i.e. 300 MJ/m²; 600 MJ/m²; 900 MJ/m²; 1200 MJ/m²; 1500 MJ/m². In EN 1991-1-2 [51], an 80% fractile value of fire load density for office occupancies corresponds to 511 MJ/m² according to the Gumbel distribution. In a recent survey
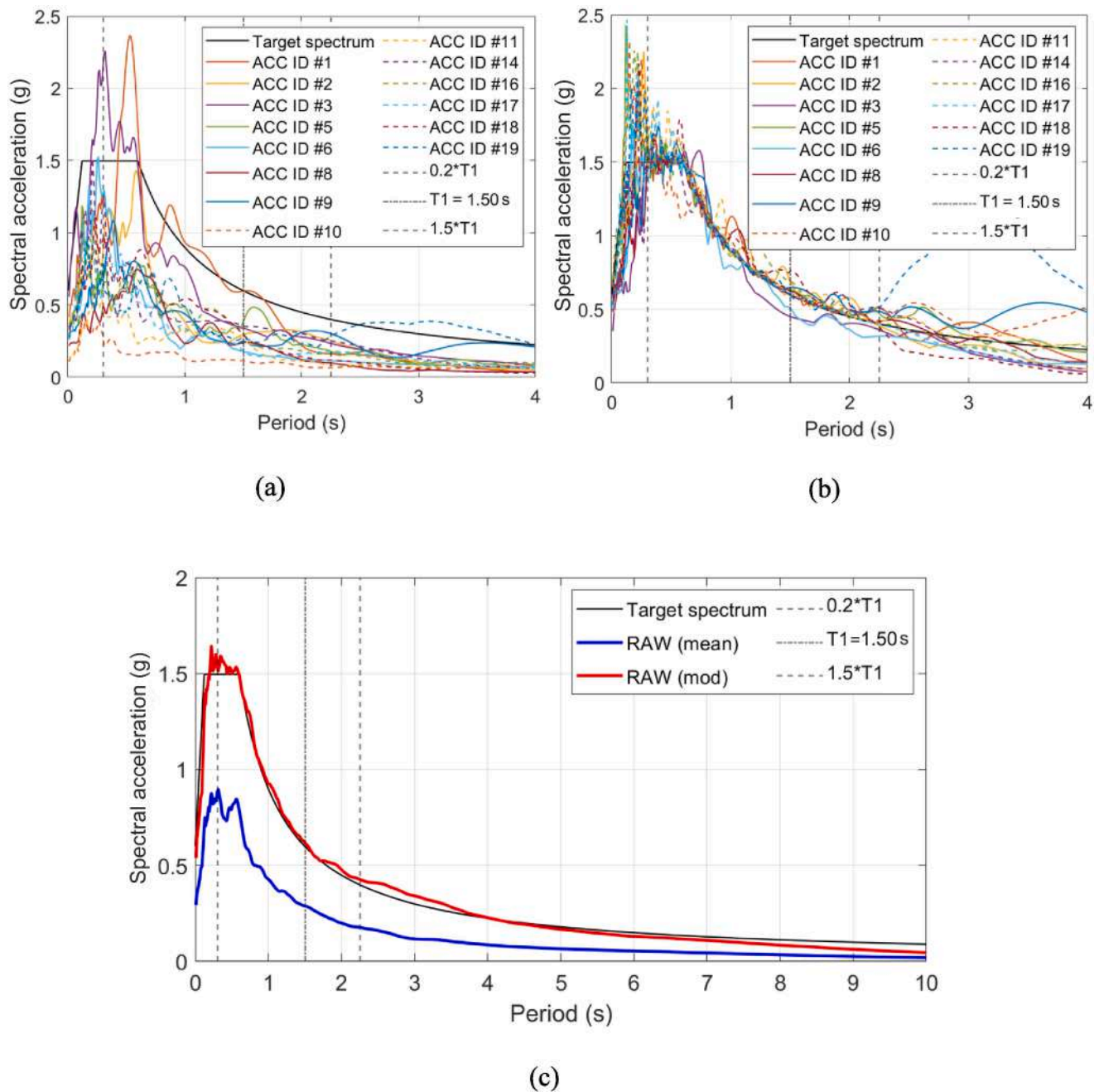
Fig. 8. Acceleration Response Spectra: (a) original, (b) scaled, (c) scaled average spectrum.

conducted in the US, the measured total fire load density, including moveable and fixed content, had a mean value of 1486 MJ/m^2 [58]. For this reason, the analyses covered fire load density values up to 1500 MJ/m^2. Fire load densities lower than 300 MJ/m^2 were deemed too low.

The prototype structure presented in the NIST report was not originally designed against fire. However, it is possible to determine the hourly ratings that would have been required for this type of building according to the U.S. guidelines, including the 2021 International Building Code (IBC) [59]. Given the initial floor area (11,523 m^2) and building height (35.4 m, 8 storeys), without considering area or height increases, the building is classified as Type IB. Moreover, since the structural steel framing is non-combustible, it complies with the requirements of Type I and Type II construction, and consequently a 2-hour fire resistance rating is required. In high-rise buildings, special

requirements for automatic sprinklers allow for modifying Type IB with Type IIA requirements, which implies a 1-hour reduction in the fire-resistance rating for both the columns and floors. Thus, the required fire resistance rating for the building can be taken as 1 h. It is possible to determine the thickness of fire protections depending on the insulation materials (i.e. insulation boards, intumescent paint, and spray-applied fire-resistive materials). However, in this work the steel members, for simplicity, were not equipped with fire protection in order to assess the framework methodology without introducing a further source of uncertainty, i.e. the damage of the fire protection owing to earthquake. It is a conservative approach not to include fire protections given the likelihood of damage to the passive fire protection during an earthquake. This aspect was left for future improvements.
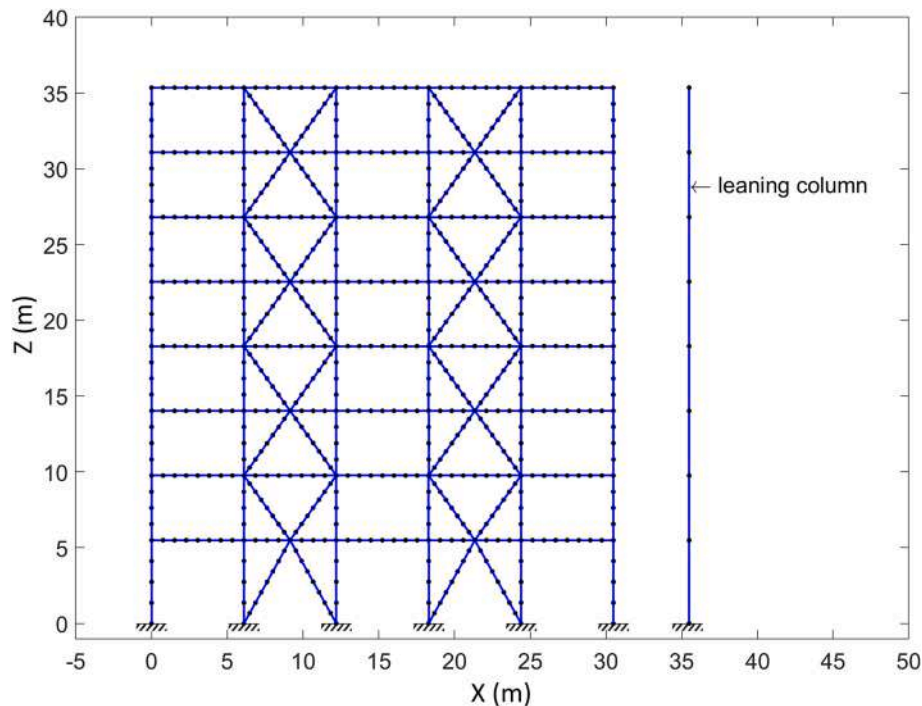
Fig. 9. Numerical model for the case study.

3.3. Numerical FE model

In order to reduce the computational time needed to perform a large number of FFE analyses, the full 3D model of the building, that includes the secondary frames and the full slab, was not considered, and the perimeter frame shown in Fig. 7 was modelled. In this respect, it is worth pointing out that the slab is not composite with the girders and consequently its effect would be minor. In general, a composite action between the girder/beam and the slab would be desirable because it would increase both strength and stiffness. Nonetheless, the slab, which acts as a heat sink, was considered when performing the thermal analysis.

The frame is modeled with nonlinear displacement-based beam-column elements using the SteelFFEThermal [33] uniaxial material. Fiber sections were selected to model the girders, columns, and braces. A sensitivity analysis was performed in order to determine the mesh size of the elements. In detail, each column was discretized with four elements, while the girders and the bracings were discretized into eight elements to accurately represent displacements, stresses, and strains in each member (see Fig. 9). Equivalent geometric imperfections were included for columns and braces to allow for geometric imperfections, e.g. member out-of-straightness, and mechanical imperfections, such as residual stresses. The magnitude of such imperfections was selected according to EN 1993-1-1 [60]. A leaning column was linked to the frame using horizontal "equalDOF" to simulate: (i) flexural continuity of the columns belonging to the gravity frames, and (ii) the P-Δ effects. The leaning column was modeled with elastic beam-column elements with a large cross section area and moment of inertia that was equal to the sum of the geometric properties of the other columns. An equivalent damping ratio of 3% was assumed for the seismic simulations.

Some modifications to the 3D frame model were required when the analysis switches from earthquake to fire. In particular, the horizontal diaphragms and the leaning column were removed after the seismic analysis was completed to allow for differential horizontal displacements of the structural members that may be subjected to fire.

The heat transfer analysis was performed after the fire development analysis in the compartment affected by fire ignition was completed in OZone. Fig. 10 shows the boundary conditions for the heat transfer

analyses of the columns, bracings, and girders taken for the case study under consideration. These boundary conditions are typical of perimeter frames.

To summarize, the analyses were performed for 14 accelerograms scaled at 6 different intensity values, 4 different values of window width, and 5 different fire load densities, as listed in Table 4. Thus, a total of 1680 simulations were performed. The Latin Hypercube Sampling (LHS) [49] was used to randomly generate the variable ε for steel retention factor $k_{y,2\%,T}$ (Eq. (1)), which was needed to calculate the yield strength at ambient and high-temperatures for each simulation. The main outcomes are described and discussed in Section 4.

4. Probabilistic analysis results

This section describes the results obtained from the 1680 simulations; in particular, one representative analysis is presented in Section 4.1 and the FFE fragility functions are derived in Section 4.2.

4.1. Numerical simulations

The simulation results were classified into several categories as shown in Fig. 11 and listed below:

- **Structure collapse due to earthquake:** The collapse of the building due to the seismic event is related to the likelihood of extensive damage to the structural elements, which can be characterized by the inter-storey drift ratio. As previously mentioned, an IDR equal to 6% was chosen as the threshold for collapse, which is three times the recommended collapse limit state value for a braced steel frame (i.e., 2% IDR) in FEMA P-356 [41]. Extensive yielding, buckling of braces, and connection failures are expected at the selected threshold. Thus, simulations with maximum inter-storey drift ratios larger than 6% were considered to experience structural collapses during the earthquake without the subsequent FFE analysis (232 out of 1680 analyses).

- **Structure collapse due to earthquake (numerical problems):** The simulation did not converge during the nonlinear time-historey
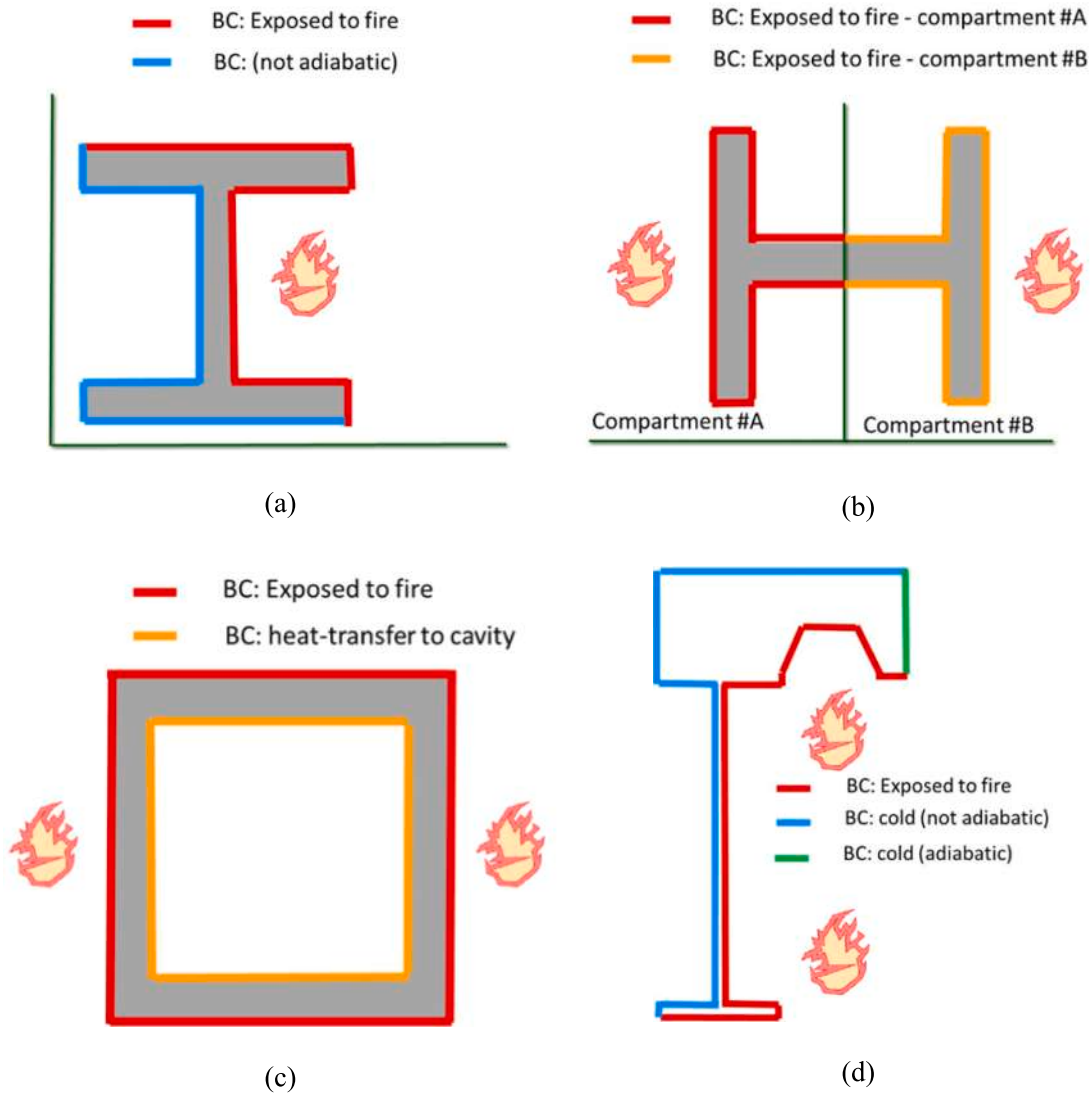
Fig. 10. Boundary conditions for thermal analysis: (a) external column, (b) column between two compartments (internal column), (c) brace, (d) girder.

Table 4
Analysis parameters.

Parameter	Values
Accelerograms	14 accelerograms
Acceleration scale factor	0.50 0.75 1.00 1.25 1.50 1.75
Window width (m)	1.5 3.0 4.5 6.0
Fire load density (MJ/m^2)	300 600 900 1200 1500

analysis. Indeed, based on the last step of the converged structural response of the two earthquake analyses, it was possible to observe high deformation on some braces and a high value of IDR indicative of structural collapse. In fact, the IDR was between three and five times the collapse limit state of 2.0% for a braced steel frame as for FEMA P-356. (2/1680 analyses).

- **No FFE event:** No FFE occurred because the thresholds for IDR and PFA were not exceeded for an ignition to happen (277/1680 analyses).
- **FFE event (girder failure first):** The FFE event occurred and at least one girder reached the failure limit state before any column failure (1123/1680 analyses).
- **FFE event (column failure first):** The FFE event occurred and at least one column reached the failure limit state before any girder

failure. For this case study, no column failure as the first structural element to experience a limit state was observed. The main reason was the low utilization factor of the columns under the FFE scenario (0/1680 analyses). In general, the low utilization factor of columns owing to the seismic design can affect the fire response of a building [61]

- **FFE event (numerical problems):** The FFE event started but the analysis was interrupted due to numerical problems before reaching the girder or column failure limit state. These simulations were discarded in the analysis of results (48/1680 analyses).

It is worth noting that about 500 simulations did not lead to an FFE event because either the ground motion was not strong enough to ignite a compartment or the ground motion was too strong that caused the collapse of the structure. Fig. 11 shows the maximum IDR as a function of the spectral acceleration (Sa) at the first period of the structure, where the results are grouped based on the above-mentioned classifications. It is interesting to note that the highest IDR values are observed in the Sa interval 0.75 g–1.25 g. Indeed, as the ground motion record is scaled up, the weak cycles in the early instances of the response become strong enough to damage the structure, whose characteristics change for the subsequent stronger cycles Vamvatsikos and Cornell [62]. Thus, lower floors may exhibit early inelastic behaviour with stronger ground
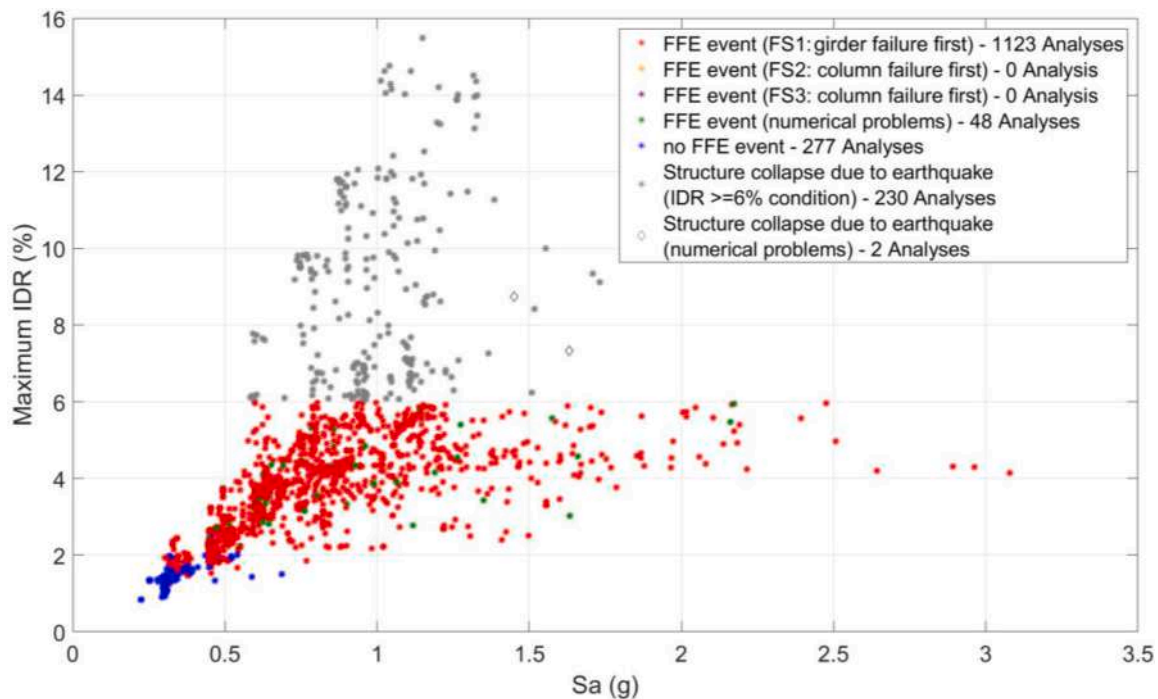
Fig. 11. Classification of the analysis results.

Table 5
Parameters of the selected analysis.

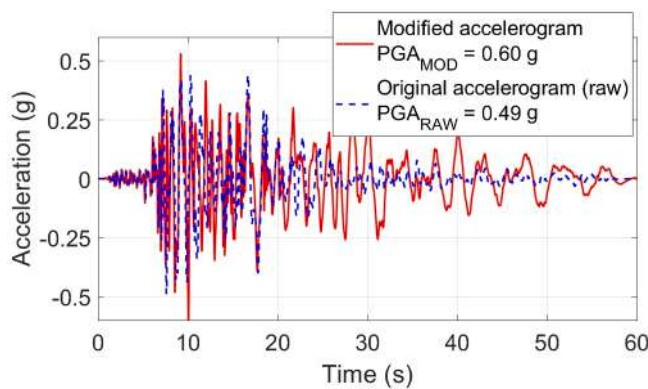| Parameter	Value
Accelerogram	Northridge, USA (ID 1)
Acceleration scale	1.00
Window width (m)	1.5
Fire load (MJ/m^2)	1500

Fig. 12. Selected accelerogram for the FFE simulation.

motions, which would reduce the vulnerability of floors located at higher levels. Hence, increasing the Sa intensity can lead to lower maximum IDR values. As expected, no FFE event was detected for low Sa values. Moreover, had been the conventional value of 2% IDR considered to identify structural collapse, very few analyses would have caused an FFE event.

One sample simulation with parameters listed in Table 5 is selected to review the results in detail. The selected seismic action was represented by a natural accelerogram (Northridge 1994), which was modified to match the target spectrum, as shown in Fig. 12. As a result, the peak ground acceleration became 0.60 g and the spectral acceleration at the first period of the structure was equal to 0.62 g. The earthquake occurred at 4:31 am, Monday, January 17, 1994, with a magnitude Mw equal to 6.7. In particular, the ground motion was recorded by the station located at Beverly Hills – 14145 Mulholland drive.

Fig. 13 illustrates the results of the numerical simulation of the nonlinear dynamic analysis for the selected ground motion. As expected, and in accordance with the capacity design philosophy, the energy dissipation was concentrated in the braces, especially in the ones located on the 4th and 5th floors, as shown in Table 6. All the columns and girders remained elastic during the seismic event. The deformed shape of the structure at the end of the earthquake is shown in Fig. 13a. The maximum IDR and PFA of each floor are illustrated in Fig. 13b, and the horizontal displacements of each floor are shown in Fig. 13c. Most of the floors exhibited IDR and PFA larger than the assumed thresholds for an FFE event to occur. The condition of the non-structural components, i.e., glazing, partition walls, and doors, are indicated by removing them from the model of the prototype building when damaged, as presented in Fig. 14a-c. For example, if a door is represented with a gray shade, it implies that the door is closed.

The bay at which the ignition occurs is randomly selected, with equal weight among the compartments within identified floors with ignition based on the maximum IDR and PFA as explained in the previous sections and as shown in Fig. 13b. In this scenario, the fire starts in multiple bays and floors: 2nd bay of the 3rd and 4th floors, 3rd bay of the 5th floor, and 4th bay of the 7th floor.

Fig. 14a-c shows the evolution of the fire within the building after 15 min, 30 min, and 45 min from the initial ignitions following the earthquake. The compartments that are shaded with red color are caught on fire and the labeled values in each compartment indicate the temperature inside the compartment at the considered time. Fig. 14d illustrates the time–temperature curves for each compartment on the 7th floor with a fuel load density of 1500 MJ/m^2. Temperatures as high as 1200 °C were recorded. The fire curves at the 1st and 5th bays are different from the other bays because the exterior bays have a different number of window panels.

The thermal field in the cross section is generally defined in Open-Sees at multiple temperature zones and they can be up to 15 zones for 3D beam-column elements, as shown in Fig. 15b and Fig. 15d. Thus, the
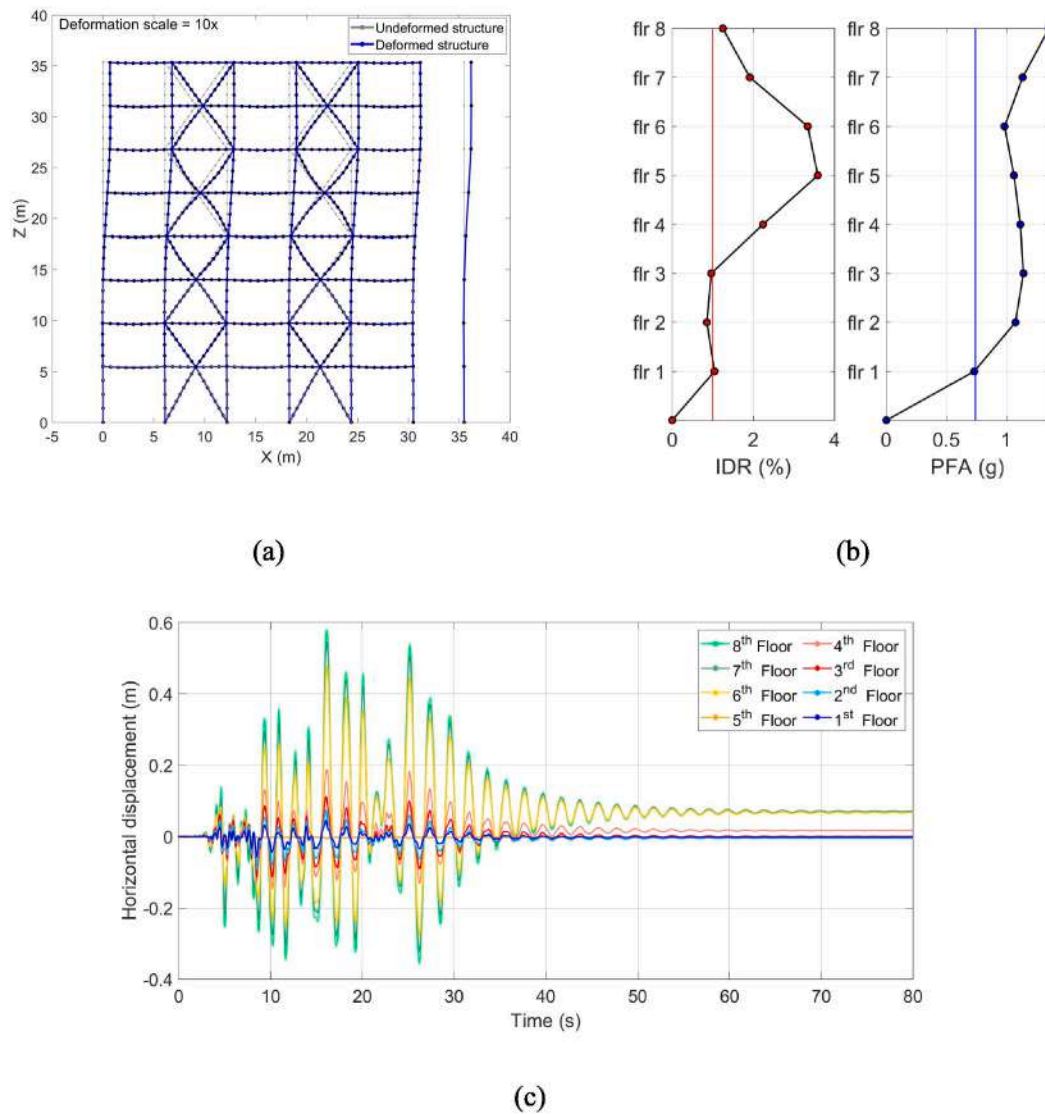
(a)

(b)

(c)

Fig. 13. (a) Deformed shape at the end of the seismic event (amplified by a factor of 10); (b) maximum inter-storey drift (IDR) and maximum peak floor acceleration (PFA); (c) horizontal displacement of the floors.

Table 6
Energy dissipation in the braces.

	Ground floor	1st floor	2nd floor	3rd floor	4th floor	5th floor	6th floor	7th floor
Energy dissipation of the braces (MJ)	0.424	0.393	0.643	0.531	2.527	1.974	0.318	0.347

MATLAB script extracts 15 temperature data zones from the thermal analyses and generates the input data for OpenSees. It is worth pointing out that the concrete slab was considered only for the thermal analyses because it was not designed as a composite slab. As highlighted in Section 3.3, the temperature distribution was not uniform in the steel sections because the girders were heated on three sides and the columns of the considered frame were located on the building boundaries.

The FFE structural analysis followed the heat transfer analysis for the selected FFE. Failure of the first structural member occurred 23 min after the start of the fire due to the excessive rate of vertical deflection in the girder located at the 6th floor and in the 3rd bay, as illustrated in Fig. 16 and Fig. 17a. Partial collapse occurred 45 min after the start of the fire due to the failure of several structural members. Fig. 17b shows the final deformed configuration of the steel frame at the end of the simulation. In

particular, despite the low utilization factor of the columns, the loss of transverse restraint owing to the girder failure caused an increase in the column effective length that eventually led to column buckling and the collapse of a portion of the building.

4.2. Fragility functions

In this section, FFE fragility functions were derived based on the 1680 simulation outcomes. A fragility function expresses the probability P that an engineering demand parameter (EDP), such as IDR or vertical displacement, exceeds a limit state (LS) conditioned on an intensity measure (IM), such as peak ground acceleration or fire load density. Fragility functions are often expressed in terms of a lognormal cumulative distribution and have the form of Eq. (6).
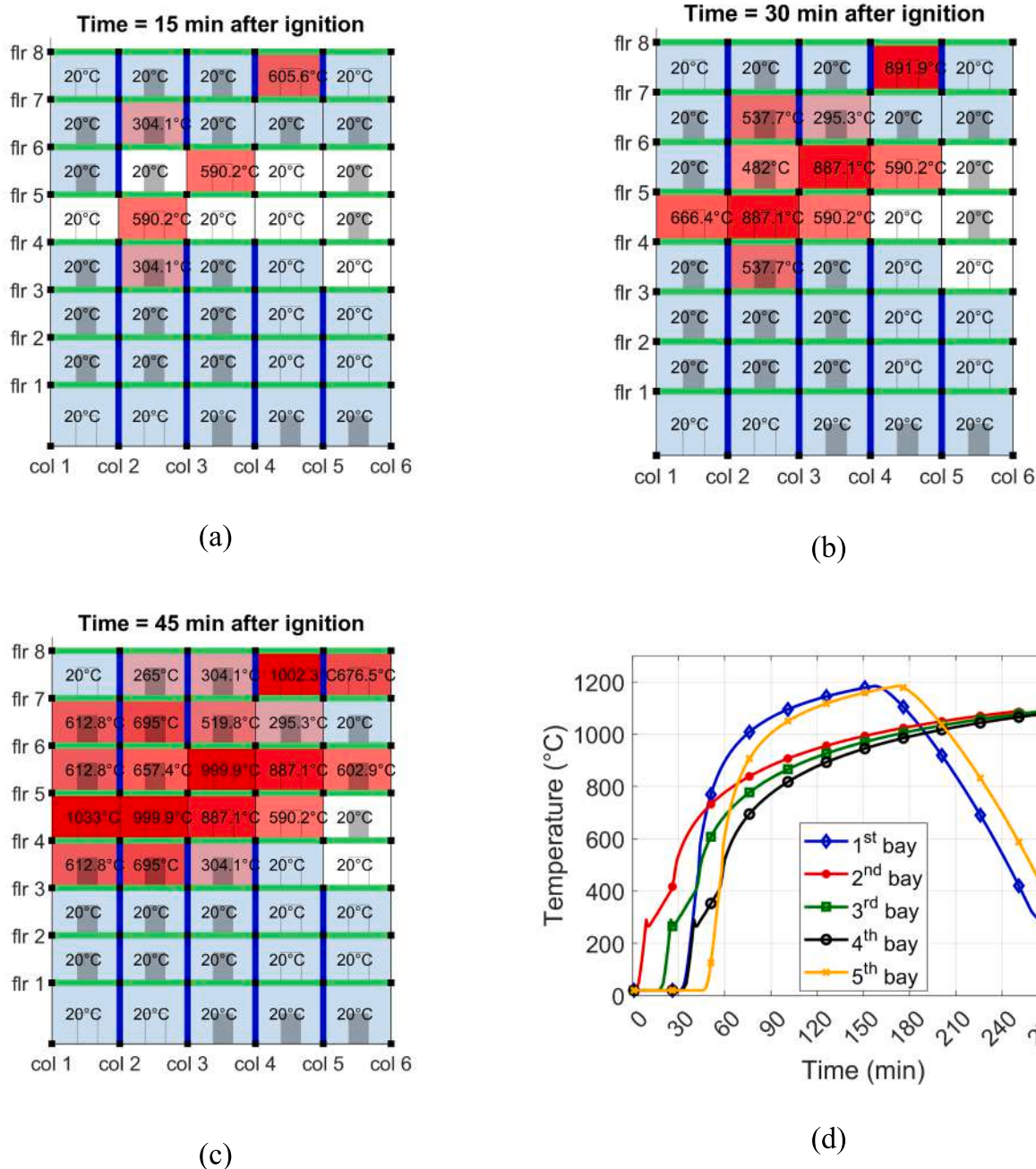
(a)

(b)

(c)

(d)

Fig. 14. Fire spread within the building after (a) 15 min, (b) 30 min, and (c) 45 min from initial ignitions after earthquake. (d) Time-temperature curve of fire for floor 7.

$$P(EDP > LS | IM = x) = \varnothing \left(\frac{\ln\left(\frac{x}{\theta}\right)}{\beta} \right) \qquad (6)$$

where $\varnothing$ is the standard normal cumulative distribution function (CDF), θ is the median of the IM and β is the standard deviation of the intensity measure. A typical EDP representing the damage induced by a seismic event is IDR, whereas in the case of an FFE, meaningful EDPs as related to structural fire engineering, such as vertical or horizontal displacements and displacement rates of structural members. A representative IM for an FFE scenario is the time to failure of a structural member that reflects the level of damage induced by the earthquake.

Many researchers studied statistical procedures for estimating parameters of fragility functions and characterizing the results of probabilistic models, especially in the seismic domain [63–72] but also in the

fire domain [26–29,31].

Three methods are commonly adapted for estimating the fragility parameters:

- Cloud analysis (CA) is based on simple regression of the structural response versus the IM using a meaningful number of ground motions.
- Incremental dynamic analysis (IDA) consists in performing nonlinear dynamic analyses by scaling an IM.
- Multiple stripe analysis (MSA) uses different suites of the IM at each pre-defined value (stripe).

All three models have been used to develop probabilistic seismic models, whilst only CA and MSA are generally used to develop probabilistic fire models [29,31]. Indeed, the IDA methodology implies the
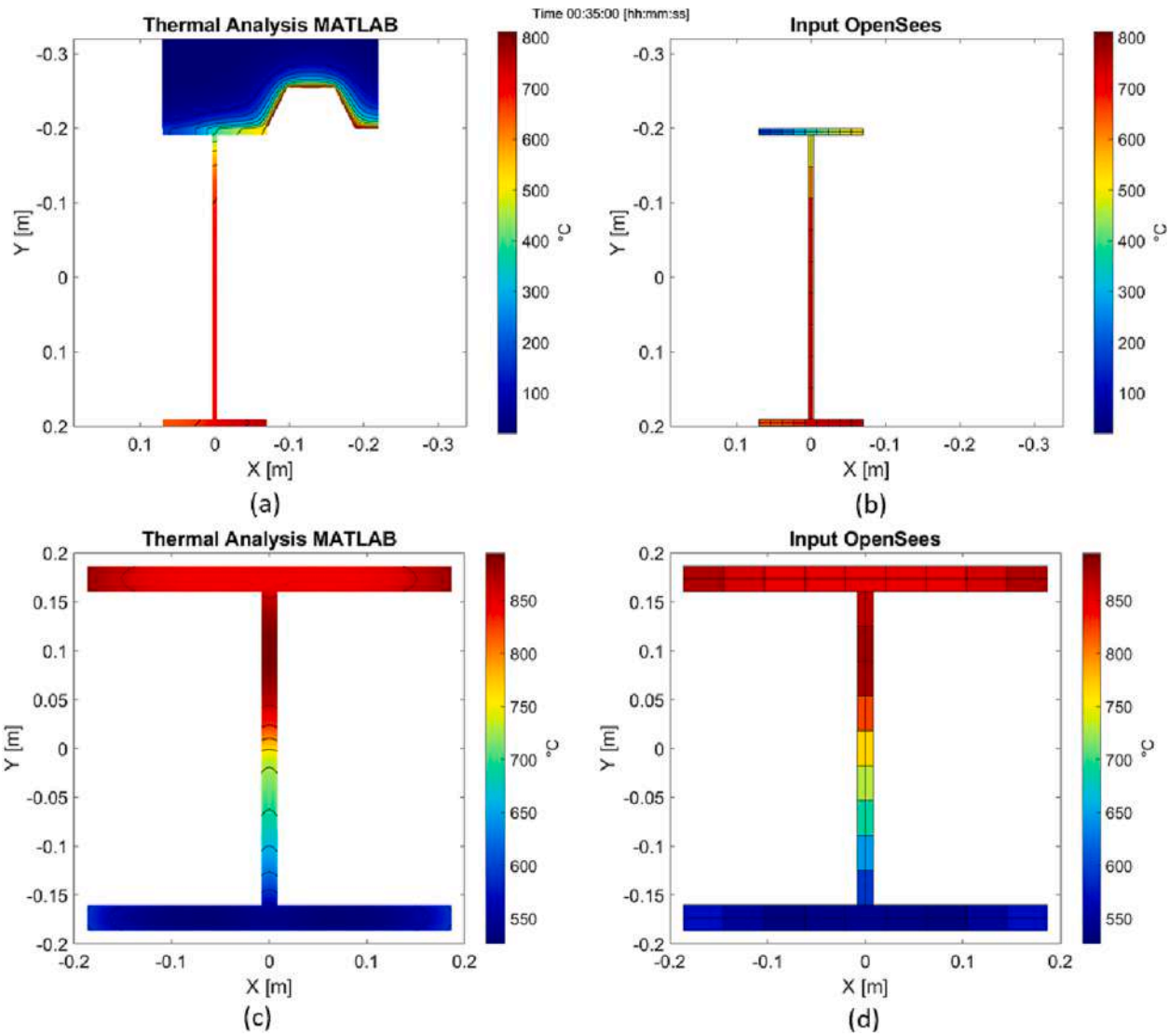
Fig. 15. Temperature distribution of structural elements in the compartment at floor 5 – bay 1 (a) W14 × 14.5 × 132 girder (MATLAB thermal model); (b) W14 × 14.5 × 132 girder (Equivalent OpenSees); (c) W16 × 5.5 × 26 column (MATLAB thermal model); (d) W16 × 5.5 × 26 column (Equivalent OpenSees).
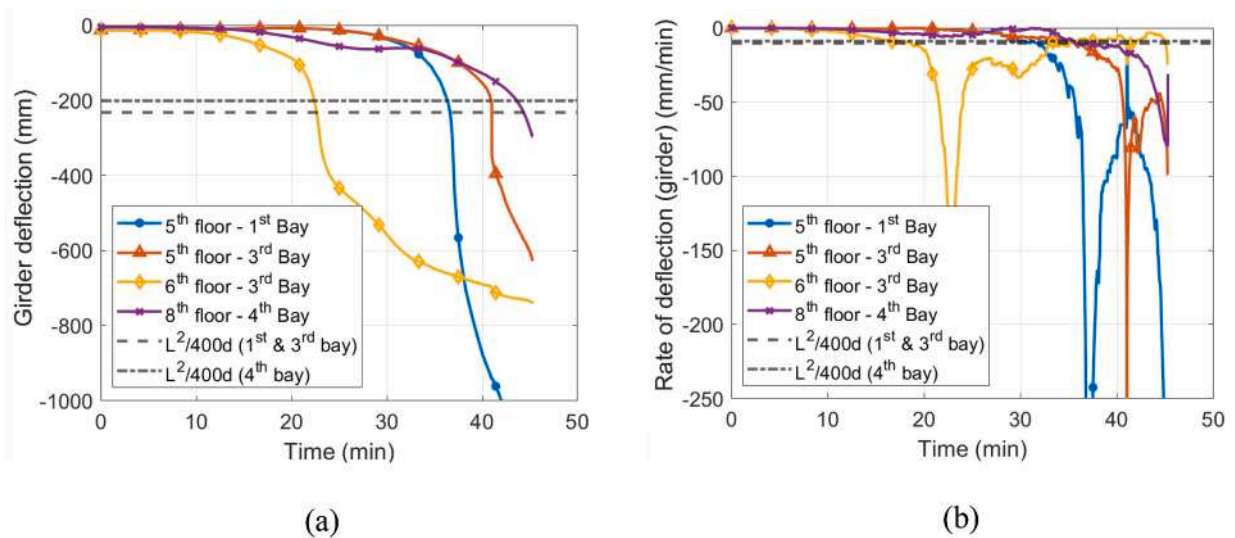

Fig. 16. Girder failure criteria: (a) deflection; (b) rate of deflection.
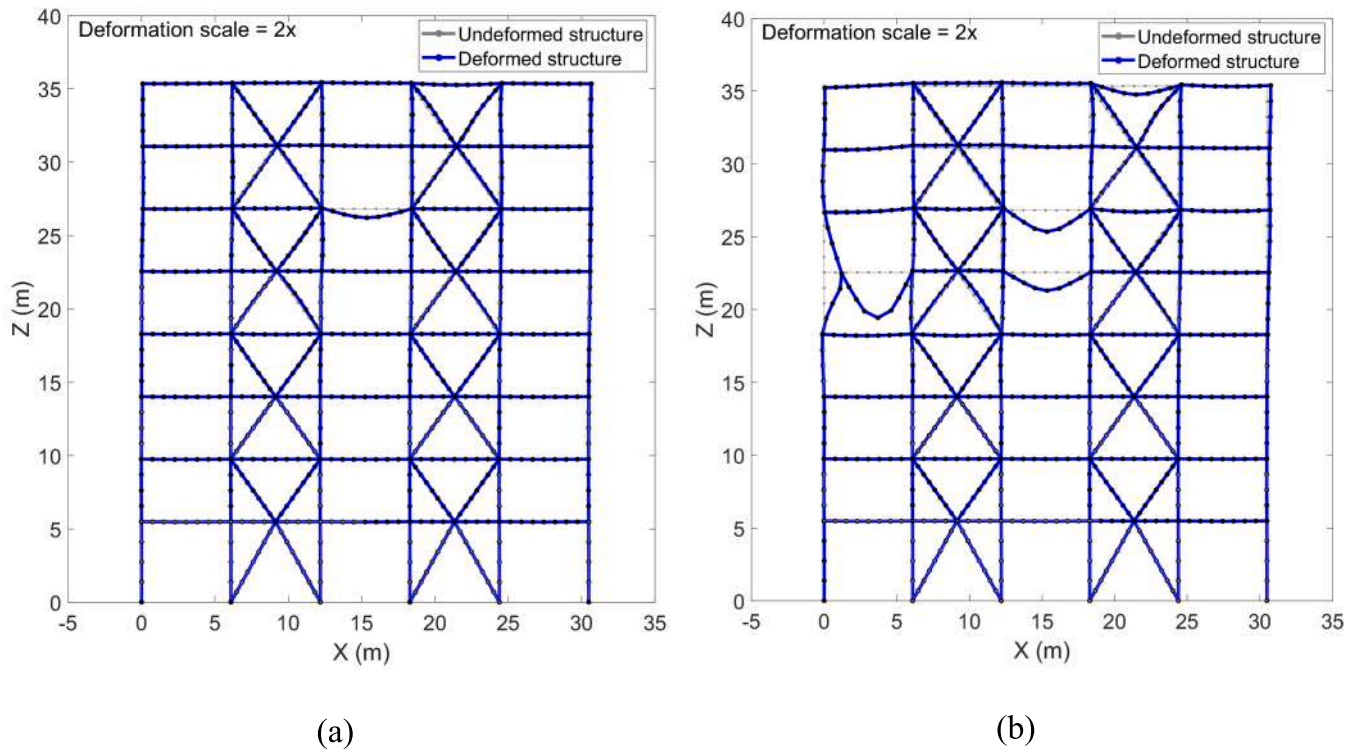
(a)

(b)

Fig. 17. Deformed shape: (a) 23 min (1st girder failure); (b) 45 min (collapse).

Table 7
Comparison of the performance of different probability distribution fits to the FFE data.

Distribution	AIC	Difference compared to Lognormal	AICc	Difference compared to Lognormal
Generalized Extreme Value	4825	−28.2 %	4817	−28.2 %
Logistic	6092	−1.5 %	6086	−1.5 %
Lognormal	6183	0 %	6177	0 %
Gamma	6411	3.7 %	6405	3.7 %
Normal	6917	11.9 %	6911	11.9 %
Weibull	7210	16.6 %	7204	16.6 %
Rayleigh	7782	25.9 %	7778	25.9 %
Extreme Value	8132	31.5 %	8126	31.5 %
Generalized Pareto	8681	40.4 %	8673	40.4 %
Exponential	9169	48.3 %	9165	48.3 %

scaling of the fire IM, such as the fire load or the heat flux, and this can quickly lead to unrealistic fire scenarios [29]. Given that the FFE models concern both seismic and fire parameters, all three methods could be in principle appropriate to develop a probabilistic FFE framework. In the following, since the accelerograms were scaled at different intensities, as shown in Table 4, an approach similar to the IDA methodology was employed to derive the FFE fragility functions [63]. In particular, by assuming a lognormal distribution, the mean and standard deviation were estimated with Eq. (7) and Eq. (8).

$$\ln\widehat{\theta} = \frac{1}{n} \sum_{i=1}^{n} \ln IM_i \tag{7}$$

$$\widehat{\beta} = \beta_{EDP|IM} = \sqrt{\frac{1}{n-1} \sum_{i=1}^{n} \left(\ln\left(\frac{IM_i}{\widehat{\theta}}\right) \right)^2} \tag{8}$$

where:

- n is the number of considered FFE events
- IM is the IM value associated with the onset of a limit state

Despite the common assumption that the EDP follows a lognormal distribution when conditioned on the IM, several other distributions were considered and compared using the Akaike information criterion (AIC) method [73,74], as reported in Table 7. The AIC is a mathematical method that evaluates and compares different possible statistical models and determines which one is the best fit for the data. The AIC method has the form of Eq. (9).

$$AIC = -2\ln L + 2k \tag{9}$$

where L and $\ln L$ are respectively the likelihood and the log-likelihood at its maximum point of the estimated model and k is the number of parameters. The use of a second-order corrected AIC (AICc) is recommended when the sample size is small compared to the number of parameters ($n/k < 40$) [75], as shown in Eq. (10):

$$AIC_c = AIC + \frac{2k^2 + 2k}{n-k-1} \tag{10}$$

where n denotes the sample size. Note that for $n \to \infty$, $AIC_c = AIC$.

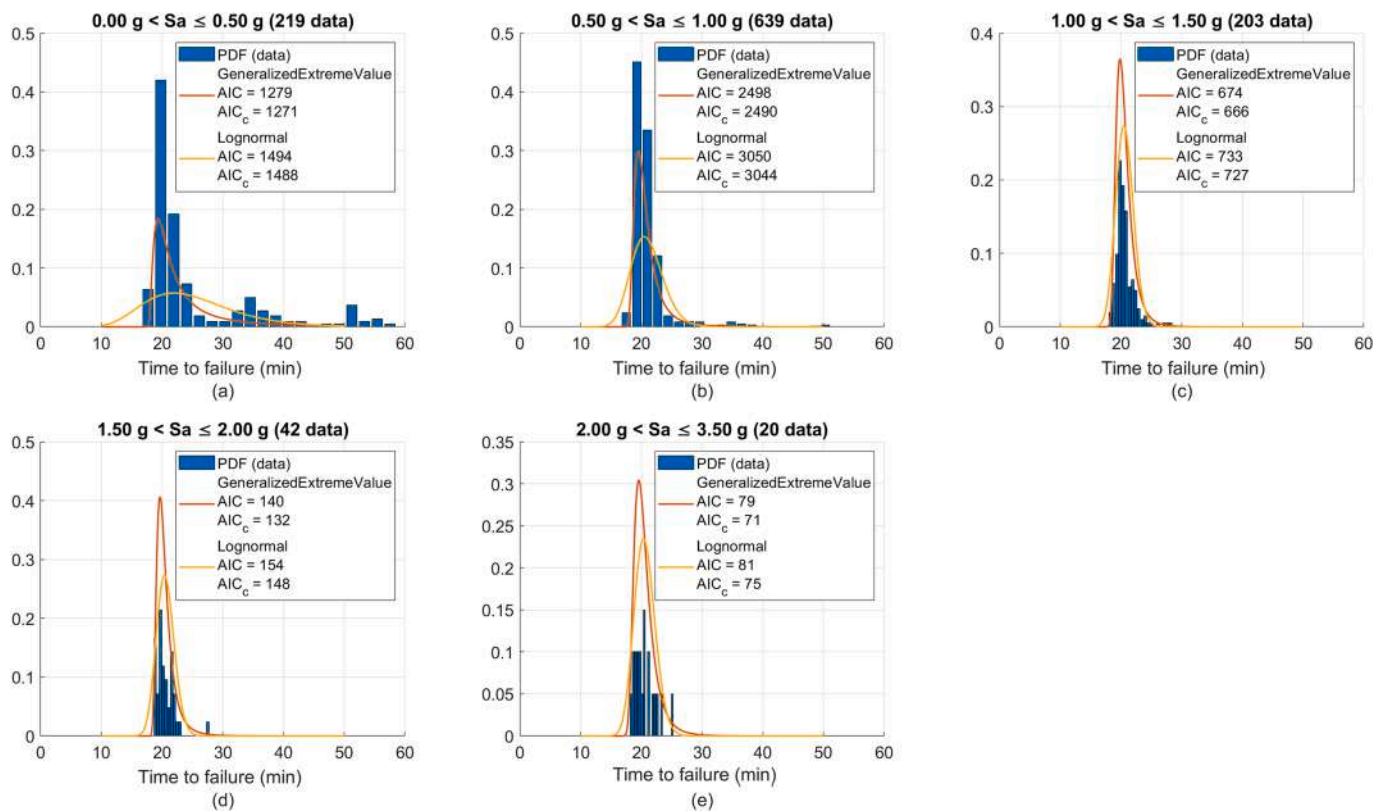AIC uses a model maximum likelihood estimation (log-likelihood) as

Fig. 18. Probability density function (PDF) of the girder failure time and function distributions.

Table 8
Median and standard deviation of the data in terms of the time to failure, grouped based on spectral acceleration.

Sa interval	Median (min)	Standard deviation (min)
0.0 g < Sa ≤ 0.5 g	21.13	9.47
0.5 g < Sa ≤ 1.0 g	20.25	3.37
1.0 g < Sa ≤ 1.5 g	20.22	1.55
1.5 g < Sa ≤ 2.0 g	20.19	1.57
2.0 g < Sa ≤ 3.5 g	20.19	1.76

Table 9
Parameters of the GEV distribution for the girder failure fragility functions with time to failure as the *IM* and grouped based on S_a.

	0.0 g < Sa ≤ 0.5 g	0.5 g < Sa ≤ 1.0 g	1.0 g < Sa ≤ 1.5 g	1.5 g < Sa ≤ 2.0 g	2.0 g < Sa ≤ 3.5 g
k	0.714	0.243	0.102	0.196	0.125
σ	2.478	1.263	1.013	0.921	1.218
μ	20.45	19.82	19.95	19.82	19.73

a measure of fit and adds a penalty term for models with higher parameter complexity to avoid overfitting. Given a set of candidate models for the data, the preferred model is the one with the minimum AIC value.

The outcome of the comparative analysis for the girder fragility functions is reported in Table 7. The results in Table 7 indicate that compared to other statistical models, the lognormal distribution can serve as a candidate distribution to define the FFE fragility functions. However, the Generalized Extreme Value (GEV) distribution showed the best fit to the data.

Fig. 18 illustrates the lognormal and the generalized extreme value probability density functions (PDF) of the fire duration that leads to girder failure due to FFE, grouped into five spectral acceleration intervals. The dispersion associated with the lognormal distribution is higher at lower spectral accelerations, especially for those less than 0.5 g, implying that the time at which the failure of the girder occurs covers a wider range. This was expected since damage in the structural and the non-structural elements has more variability at lower values of the seismic intensity, which affects the spread of the fire and the possible number of multiple ignitions. Conversely, when the seismic intensity increases, the damage tends to be more uniform across the building and consequently, the ignitions and the fire spread vary in less extent. The same reasoning applies to the PDF for the GEV distribution, but as indicated by the AIC values, the distribution provides a better fit to the

data. The aforementioned observations are highlighted in Table 8, where the median and standard deviation of the data for each spectral acceleration interval are summarized. It can be observed that lower values of spectral acceleration correspond to a higher dispersion of the time to failure of the girder, i.e., the standard deviation of 9.5 min is largest at Sa less than 0.5 g, whereas the median values remain unchanged and equal to about 20 min.

Based on the results of the comparative analysis, the GEV distribution was selected to derive the fragility functions. Not only the distribution provides the best fit, but also can be represented in a simple and closed form function with three parameters. The cumulative probability distribution function for the GEV distribution has the form of Eq. (11).

$$P(EDP > LS | IM = x)$$

$$= \begin{cases} \exp\left\{ - \left[1 + k\left(\frac{x - \mu}{\sigma} \right) \right]^{-1/k} \right\} & if \ k \neq 0 \\ \exp\left\{ - \exp\left[- \left(\frac{x - \mu}{\sigma} \right) \right] \right\} & if \ k = 0 \end{cases} \tag{11}$$

where σ denotes the scale parameter (statistical dispersion of the probability distribution), μ is the location parameter (shift of the distribution) and k is the shape parameter. The shape parameter k is used to represent three different distribution families:
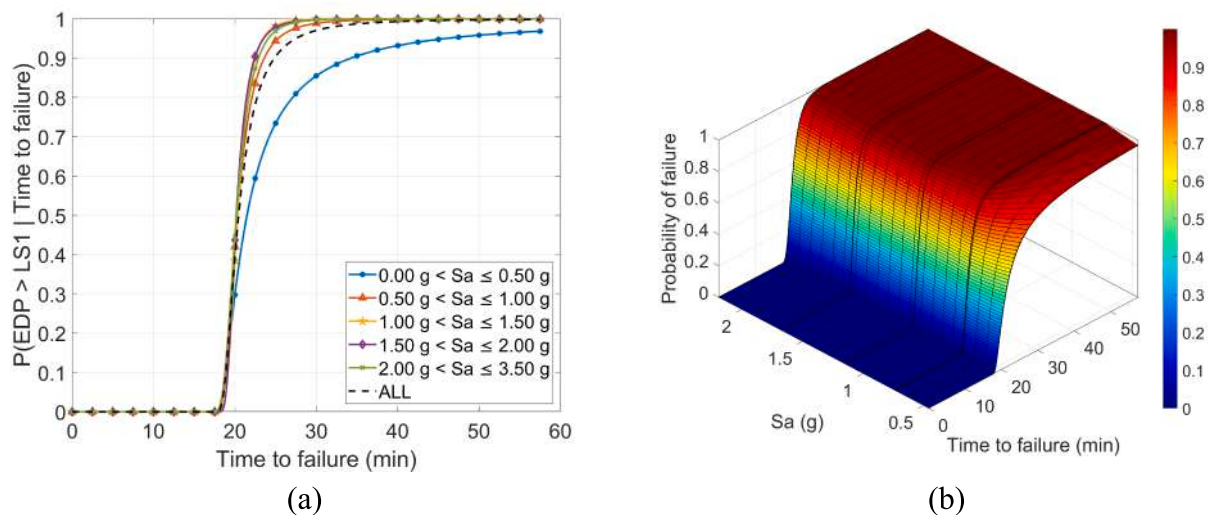
Fig. 19. a) Fragility curves for the girder limit state as a function of Sa; (b) fragility surface for the girder limit state as a function of Sa.
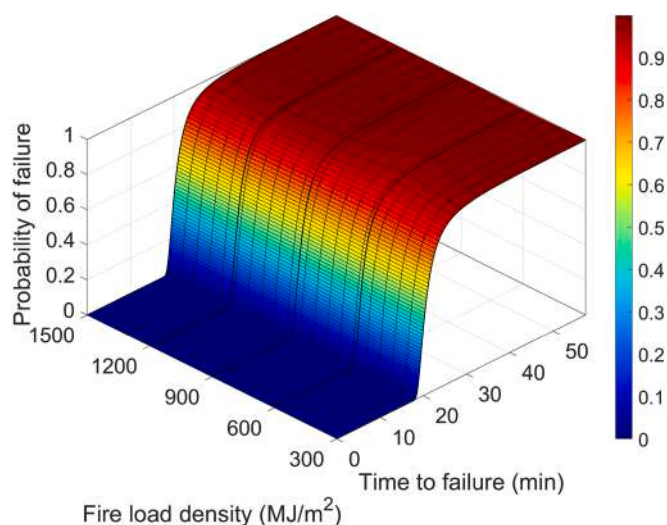

Fig. 20. Fragility surface for the girder limit state as a function of the fire load density and time to failure.

- Type I (k = 0): the GEV distribution is equivalent to the Gumbel distribution whose tails decrease exponentially, such as the normal distribution.
- Type II (k > 0): the GEV distribution is equivalent to the Fréchet distribution, whose tails decrease as a polynomial, such as Student's t-distribution.
- Type III (k < 0): the GEV distribution is equivalent to the reversed Weibull distribution, whose tails are finite, such as the beta distribution.

The shape value *k* is always above 0 for the case study analysed in this work (see Table 9); thus, the GEV Type II was used for the fragility functions.

Fig. 19a and Fig. 19b show the fragility curves and surfaces, respectively, for the girder failure conditioned on the time to failure and grouped as a function of the Sa at the first period of the structure. Fig. 19a indeed illustrates different slices of Fig. 19b. Fig. 19 depicts that the probability of exceeding a girder failure limit state is negligible up to 18 min, followed by a sharp increase with 90% probability at 24 min. Moreover, and as expected, Fig. 19 highlights a higher probability of exceedance of reaching the girder limit state with shorter times to failure

when the structure is subjected to higher values of spectral acceleration. Indeed, for values of Sa less than 0.5 g, there is a 90% probability of exceedance of reaching the girder limit state in 33 min, whereas the limit state is reached in 22 min for the same probability target at larger Sa values. It is worth noting that for this case study, the critical steel temperature of a member does not provide valuable information. This is mainly because the girders (and the columns) are not damaged by the earthquake and are less sensitive to the overall damage to the structure. Indeed, the seismic damage induces a residual deformed shape that amplifies second order effects, which affect more the columns and not the girders, but the columns in this case study have a low utilization factor.

Fig. 20 shows the fragility surface for the probability of exceedance of reaching the girder limit state as a function of the fire load density and time to failure. It can be observed that the fire load density does not have a significant effect on the probability of reaching the limit state, because even low fire load density values with different ventilation conditions and compartment boundaries were able to induce gas temperatures in the compartment high enough to cause the failure of one girder at similar times. This can be explained by the fact that girders are unprotected and hinged at their ends. The median and standard deviation of failure time for all fire load density values are 21 min and 8 min.

It should be noted that selecting a sufficient measure of hazard to develop the fragility curves requires attention to the characteristics of the hazard. A combination of fire load density and time to failure is selected to ensure that the effect of fire scenario (short-duration high-temperature fire versus long-duration low-temperature fire) is captured on the structural response.

Finally, it is interesting to show fragility curves that are related to the residual state of the structure after the seismic event. In this respect, Fig. 21a compares the fragility curves that describe the probability of reaching the girder limit state conditioned on the time to failure and the maximum residual inter-storey drift ratio (RIDR) over all floors. The difference in the median of the two fragility curves with RIDR less than and larger than 1.0% is 0.5 min; however, the case with RIDR less than 1.0% has a larger dispersion with time to failure ranging from 17.6 to 57.5 min. As already highlighted, damage in the non-structural elements reduces the failure time. The girder failure time for the majority of cases with RIDR larger than 1% is less than 25 min. Also, the difference in the median of the failure time for the girder and the first column that follows the girder failure is about 4.5 min, as shown in Fig. 21b. The column failure does not necessarily occur in the same compartment where the girder fails but in all cases, the girder fails before the column.
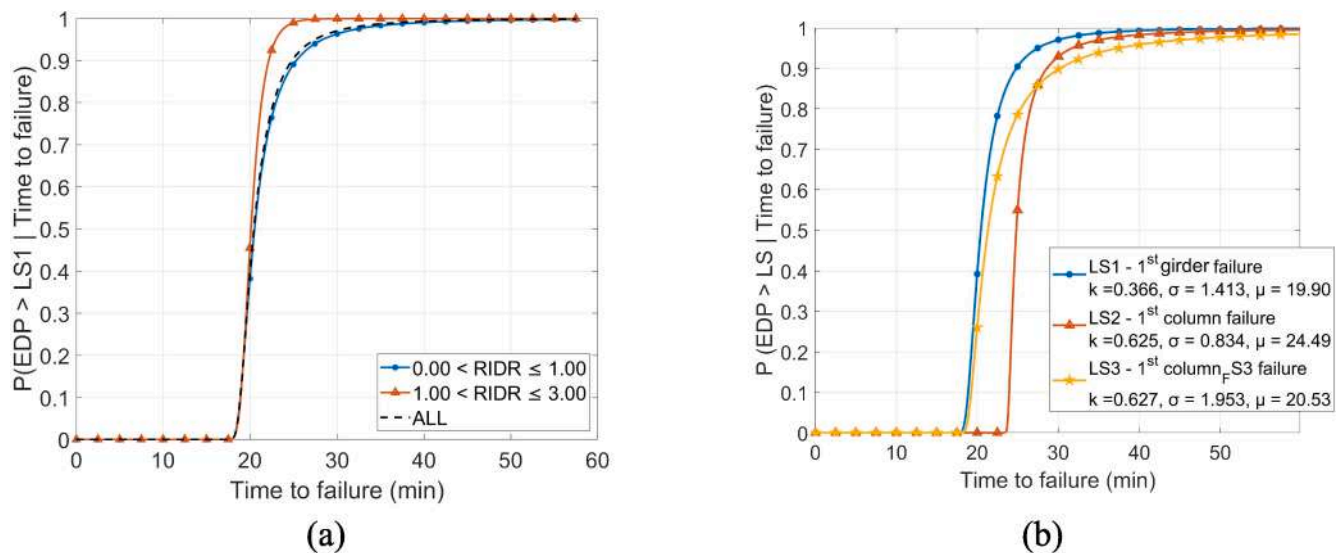
Fig. 21. (a) Fragility curve for girder failure time and as a function of residual inter-storey drift (RIDR), (b) comparison of the girder and column failure times.

5. Conclusions

The paper describes the development of a novel fire following earthquake probabilistic framework applied to a steel braced frame. For simplicity, the frame was not considered fire protected. The framework includes uncertainties related to the seismic input, the structural capacity at ambient and elevated temperatures, the fire load density and ventilation conditions, and the post-earthquake status of fire compartmentation considering the damage to partition walls, glazing, and doors. A decision tree algorithm was developed to establish the probability of ignition in the compartments within the building after the seismic event. The probability of ignition was related to the inter-storey drift ratio and peak floor acceleration.

The results showed that about 500 analyses, out of 1680 randomly generated cases, did not experience FFE events because either the ground motion was not strong enough to induce large enough damage that could ignite a fire or the structure experienced collapse owing to the seismic event. In cases with FFE, girders were always the first element to fail given that they were unprotected and hinged at ends. The median value of time to reach the girder limit state was about 20 min. The failure time for the girders in scenarios with smaller spectral acceleration intervals exhibited the highest dispersion because the structural and the non-structural damage had more variability, which affected the spread of the fire and the possible number of multiple ignitions in the building. Moreover, the higher the spectral acceleration, the higher the probability of exceeding an FFE limit state for a shorter time to failure. The fire load density did not have a significant impact on the failure time because the gas temperatures in the compartments were high enough, even for low fire load density values, to cause the failure of one girder at similar times. The generalized extreme value type II distribution was found the most suitable distribution to characterize the FFE fragility functions given that it provided the best data fit with a simple closed-form formulation to be used in practice. It may be observed that an actual building of such occupancy and characteristics entails a fire resistance rating of 1 h and failure times calculated in this paper are expected to increase given the fact that the seismic damage to the fire protection would not be of such extent to leave the frame completely unprotected. Moreover, the seismic damage to members and fire protections would be mostly localized in the bracings. In this respect, future works will be addressed to include the effect of the damage to passive fire protection and to consider other structural systems, such as moment-resisting frames.

Declaration of Competing Interest

The authors declare that they have no known competing financial interests or personal relationships that could have appeared to influence the work reported in this paper.

Data availability

Data will be made available on request.

Acknowledgements

References

[1] Elhami Khorasani N, Garlock MEM. Overview of fire following earthquake: historical events and community responses. Int J Disaster Resil Built Environ 2017; 8(02):158–74.

[2] Scawthorn C, Eidinger JM, Schiff AJ. Fire following earthquake. Technical Council on Lifeline Earthquake Engineering Monograph, No. 26. American Society of Civil Engineers; 2005.

[3] Sarreshtehdari A, Elhami-Khorasani N, Coar M. A streamlined approach for evaluating postearthquake performance of an electric network. Sustain Resil Infrastruct 2020;5(4):232–51.

[4] Sarreshtehdari A, Elhami Khorasani N. Integrating the fire department response within a fire following earthquake framework for application in urban areas. Fire Saf J 2021;124:103397. https://doi.org/10.1016/j.firesaf.2021.103397.

[5] Sarreshtehdari A, Elhami-Khorasani N. Post-earthquake emergency response time to locations of fire ignition. J Earthq Eng 2022;24(4):1–28.

[6] Mousavi S, Bagchi A, Kodur VKR. Review of post-earthquake fire hazard to building structures. Can J Civ Eng 2008;35(7):689–98.

[7] EQE. The January 17, 1995 Kobe earthquake. An EQE Summary Report. EQE International; 1995.

[8] Himoto K. Comparative analysis of post-earthquake fires in Japan from 1995 to 2017. Fire Technol 2019;55(3):935–61.

[9] Taylor J. Post earthquake fire in tall buildings and the New Zealand code. Research project report. Christchurch, New Zealand: University of Canterbury; 2003.

[10] Talebi E, Tahir MM, Zahmatkesh F, Kueh AB, Said AM. Fire resistance of a damaged building employing buckling restrained braced system. Adv Steel Constr 2018;14(1):1–21.

[11] Della Corte G, Landolfo R, Mazzolani FM. Post earthquake fire resistance of moment resisting steel frames. Fire Saf J 2003;38(7):593–612.

[12] Miano A, de Silva D, Compagnone A, Chiumiento G. Probabilistic seismic and fire assessment of an existing reinforced concrete building and retrofit design. Struct Eng Mech 2020;74(4):481–94.

[13] Memari M, Mahmoud M, Ellingwood B. Post-earthquake fire performance of moment resisting frames with reduced beam section connections. J Constr Steel Res 2014;103:215–29.

[14] Behnam B, Ronagh HR. Post-earthquake fire performance-based behavior of unprotected moment resisting 2D steel frames. KSCE J Civ Eng 2015;19(1):274–84.

[15] Khorasani NE, Garlock MEM, Quiel SE. Modeling steel structures in OpenSees: Enhancements for fire and multi-hazard probabilistic analyses. Comput Struct 2015;157:218–31.

[16] Sinaie S, Heidarpour A, Zhao XL. Stress–strain–temperature relation for cyclically-damaged structural mild steel. Eng Struct 2014;77:84–94.

[17] Braxtan NL, Pessiki SP. Postearthquake fire performance of sprayed fire-resistive material on steel moment frames. J Struct Eng 2011;137(9):946–53.

[18] Keller WJ, Pessiki SP. Effect of earthquake-induced damage to spray-applied fire-resistive insulation on the response of steel moment-frame beam-column connections during fire exposure. J Fire Prot Eng 2012;22(4):271–99.

[19] Pucinotti R, Bursi OS, Demonceau JF. Post-earthquake fire and seismic performance of welded steel–concrete composite beam-to-column joints. J Constr Steel Res 2011;67(9):1358–75.

[20] Pucinotti R, Bursi OS, Franssen J-M, Lennon T. Seismic-induced fire resistance of composite welded beam-to-column joints with concrete-filled tubes. Fire Saf J 2011;46(6):335–47.

[21] Kamath P, Sharma UK, Kumar V, Bhargava P, Usmani A, Singh B, et al. Full-scale fire test on an earthquake-damaged reinforced concrete frame. Fire Saf J 2015;73:1–19.

[22] Meacham BJ. Post-earthquake fire performance of buildings: summary of a large-scale experiment and conceptual framework for integrated performance-based seismic and fire design. Fire Technol 2016;52(4):1133–57.

[23] Pantoli E, Chen MC, Wang X, Astroza R, Ebrahimian H, Hutchinson TC, et al. Full-scale structural and nonstructural building system performance during earthquakes: Part II – NCS damage states. Earthq Spectra 2016;32(2):771–94.

[24] Moehle J, Deierlein GG. A framework methodology for performance-based earthquake engineering. In Proceedings of the 13th world conference on earthquake engineering 2004. (pp. 3812-3814), August 1-6, Vancouver, Canada.

[25] Elhami-Khorasani N, Garlock M, Gardoni P. Probabilistic performance-based evaluation of a tall steel moment resisting frame under post-earthquake fires. J Struct Fire Eng 2016;7(3):193–216.

[26] Gernay T, Elhami-Khorasani N, Garlock M. Fire fragility curves for steel buildings in a community context: A methodology. Eng Struct 2016;113:259–76.

[27] Gernay T, Elhami-Khorasani N, Garlock M. Fire fragility functions for steel frame buildings: sensitivity analysis and reliability framework. Fire Technol 2019;55(4):1175–210.

[28] Lange D, Devaney S, Usmani A. An application of the PEER performance based earthquake engineering framework to structures in fire. Eng Struct 2014;66:100–15.

[29] Shrivastava M, Abu AK, Dhakal RP, Moss PJ. Severity measures and stripe analysis for probabilistic structural fire engineering. Fire Technol 2019;55(4):1147–73.

[30] Cornell CA, Krawinkler H. Progress and challenges in seismic performance assessment. Peer Cent News 2000;3(2):1–3.

[31] Randaxhe J, Popa N, Tondini N. Probabilistic fire demand model for steel pipe-racks exposed to localised fires. Eng Struct 2021;226:111310. https://doi.org/10.1016/j.engstruct.2020.111310.

[32] Memari M, Mahmoud H. Framework for a performance-based analysis of fires following earthquakes. Eng Struct 2018;171:794–805.

[33] Covi P. Multi-hazard analysis of steel structures subjected to fire following earthquake, Doctoral dissertation. University of Trento; 2021. 10.15168/11572_313383.

[34] CEN (2005): EN 1993-1-2 Eurocode 3: Design of steel structures - Part 1-2: General rules - Structural fire design.

[35] Elhami-Khorasani N, Gardoni P, Garlock M, Probabilisticfire analysis: material models and evaluation of steel structural members, J Struct Eng, 2015; 141(12): 04015050.

[36] Qureshi R, Ni S, Elhami-Khorasani N, Van Coile R, Hopkin D, Gernay T. Probabilistic models for temperature-dependent strength of steel and concrete. J Struct Eng 2020;146(6):04020102.

[37] McKenna F. Opensees: a framework for earthquake engineering simulation. Comput Sci Eng 2011;13(4):58–66.

[38] Cadorin JF, Franssen JM. A tool to design steel elements submitted to compartment fires—OZone V2. Part 1: pre-and post-flashover compartment fire model. Fire Saf J 2003;38(5):395–427.

[39] MATLAB Release 2021b, Natick, Massachusetts: The MathWorks Inc (2021).

[40] Ueno J, Takada S, Ogawa Y, Matsumoto M, Fujita S, Hassani N, Ardakani FS, Research and development on fragility of components for the gas distribution system in greater Tehran, Iran. In Conference Proceedings, in Proc. 13th WCEE, Vancouver, BC Canada, Paper, no. 193 (2004).

[41] Federal Emergency Management Agency (FEMA). Prestandard and commentary for the seismic rehabilitation of buildings. Document FEMA P-356 2000.

[42] Federal Emergency Management Agency (FEMA). Next-generation methodology for seismic performance assessment of buildings. Prepared by the Applied Technology Council for the Federal Emergency Management Agency, Report No. FEMA P-58, Washington, D.C. (2012).

[43] Federal Emergency Management Agency (FEMA). Architectural Glass Seismic Behavior Fragility Curve Development. Background Document FEMA P-58/BD-3.9.1. Submitted to the Applied Technology Council, prepared for FEMA, Washington, D.C. (2011a).

[44] American Architectural Manufacturers Association (AAMA). Recommended Dynamic Test Method for Determining the Seismic Drift Causing Glass Fallout from a Wall System, AAMA 501.6-09, Schaumburg, IL. (2009).

[45] Federal Emergency Management Agency (FEMA). Seismic Fragility of Building Interior Cold-Formed Steel Framed Gypsum Partition Walls. Background Document FEMA P-58/BD-3.9.2. Submitted to the Applied Technology Council, prepared for FEMA, Washington, D.C. (2011b).

[46] Federal Emergency Management Agency (FEMA). Seismic Fragility of Building Interior Doors. Background Document FEMA P-58/BD-3.9.3. Submitted to the Applied Technology Council, prepared for FEMA, Washington, D.C. (2011c).

[47] Calayir M, Selamet S, Wang YC. Post-earthquake fire performance of fire door sets. Fire Saf J 2022;130:103589.

[48] Sarreshtehdari A. The impact of fire following earthquake on urban environment considering the seismic performance of infrastructure networks. PhD dissertation. Buffalo: University at Buffalo; 2021.

[49] Olsson A, Sandberg G, Dahlblom O. On Latin hypercube sampling for structural reliability analysis. Struct Saf 2003;25(1):47–68.

[50] Higham NJ. Computing a nearest symmetric positive semidefinite matrix. Linear Algebra Appl 1988;103:103–18.

[51] CEN (2002): EN 1991-1-2 Eurocode 1: Actions on structures - Part 1-2: General actions - Actions on structures exposed to fire.

[52] CEN (2005): EN 1992-1-2 Eurocode 2: Design of concrete structures - Part 1-2: General rules - Structural fire design.

[53] EN 1363-1 (2020): Fire resistance tests - Part 1: General requirements.

[54] Harris JL, Speicher MS. Assessment of first generation performance-based seismic design methods for new steel buildings volume 2: Special concentrically braced frames. (National Institute of Standards and Technology, Gaithersburg, MD), NIST Technical Note. 2015, vol. 2, pp. 1863–2.

[55] ASCE 7-10. Minimum design loads for buildings and other structures. American Society of Civil Engineers; 2010.

[56] Federal Emergency Management Agency (FEMA) (2008): FEMA P-695, Quantification of Building Seismic Performance Factors.

[57] Kircher C, Deierlein G, Hooper J, Krawinkler H, Mahin S, Shing B, et al., Evaluation of the fema p-695 method-ology for quantification of building seismic performance factors. 2010.

[58] Elhami-Khorasani N, Salado Castillo JG, Saula E, Josephs T, Nurlybekova G, Gernay T. Application of a digitized fuel load surveying methodology to office buildings. Fire Technol 2021;57(1):101–22.

[59] International Code Council. International building code. International Code Council; 2020.

[60] CEN (2005): EN 1993-1-1 Eurocode 3: Design of steel structures. Part 1-1: general rules and rules for buildings.

[61] Possidente L, Weiss A, de Silva D, Pustorino S, Nigro E, Tondini N. Fire safety engineering principles applied to a multi-storey steel building. Proc Inst Civil Eng-Struct Build 2021;174(9):725–38.

[62] Vamvatsikos D, Cornell CA. Incremental dynamic analysis. Earthq Eng Struct Dyn 2002;31(3):491–514.

[63] Baker JW. Efficient analytical fragility function fitting using dynamic structural analysis. Earthq Spectra 2015;31(1):579–99.

[64] Zareian F, Krawinkler H. Assessment of probability of collapse and design for collapse safety. Earthq Eng Struct Dyn 2007;36(13):1901–14.

[65] Jalayer F. Direct probabilistic seismic analysis: implementing non-linear dynamic assessments. Ph.D. Thesis. Stanford, CA: Department of Civil and Environmental Engineering, Stanford University; 2003.

[66] Kennedy RP, Ravindra MK. Seismic fragilities for nuclear power plant risk studies. Nucl Eng Des 1984;79(1):47–68.

[67] Kim S-H, Shinozuka M. Development of fragility curves of bridges retrofitted by column jacketing. Probab Eng Mech 2004;19(1-2):105–12.

[68] Calvi GM, Pinho R, Magenes G, Bommer JJ, Restrepo-Vélez LF, Crowley H. Development of seismic vulnerability assessment methodologies over the past 30 years. ISET J Earthq Technol 2006;43:75–104.

[69] Villaverde R. Methods to assess the seismic collapse capacity of building structures: State of the art. J Struct Eng 2007;133(1):57–66.

[70] Porter K, Kennedy R, Bachman R. Creating fragility functions for performance based earthquake engineering. Earthq Spectra 2007;23(2):471–89.

[71] Shafei B, Zareian F, Lignos DG. A simplified method for collapse capacity assessment of moment-resisting frame and shear wall structural systems. Eng Struct 2011;33(4):1107–16.

[72] Tondini N, Zanon G, Pucinotti R, Di Filippo R, Bursi OS. Seismic performance and fragility functions of a 3D steel-concrete composite structure made of high-strength steel. Eng Struct 2018;174:373–83.

[73] Akaike H. Information theory and an extension of the maximum likelihood principle. In: Selected papers of Hirotugu Akaike. New York, NY: Springer; 1998. p. 199–213.

[74] Akaike H. A new look at the statistical model identification. IEEE Trans Autom Control 1974;19(6):716–23.

[75] Burnham KP, Anderson DR. Practical use of the information-theoretic approach. In: Burnham KP, Anderson DR, editors. Model selection and inference. New York, NY: Springer New York; 1998. p. 75–117.

[76] Center for Computational Research, University at Buffalo, 2022. http://hdl.handle.net/10477/79221.